

Ref. FLAVOUR(267104)-ERC-15

Ref. SISSA 10/2012/EP

Ref. TUM-HEP 837/12

Ref. CFTP/12-007

The $\mu - e$ Conversion in Nuclei, $\mu \rightarrow e\gamma$, $\mu \rightarrow 3e$ Decays and TeV Scale See-Saw Scenarios of Neutrino Mass Generation

D. N. Dinh^{a,b}, A. Ibarra^c, E. Molinaro^d and S. T. Petcov^{a,e} ¹

^a*SISSA and INFN-Sezione di Trieste,
Via Bonomea 265, 34136 Trieste, Italy.*

^b*Institute of Physics, 10 Dao Tan, Hanoi, Vietnam.*

^c*Physik-Department T30d, Technische Universität München,
James-Frank-Straße, 85748 Garching, Germany.*

^d*Centro de Física Teórica de Partículas,
Instituto Superior Técnico, Technical University of Lisbon,
1049-001, Lisboa, Portugal.*

^e*Kvali IPMU, University of Tokyo (WPI), Tokyo, Japan.*

Abstract

We perform a detailed analysis of lepton flavour violation (LFV) within minimal see-saw type extensions of the Standard Model (SM), which give a viable mechanism of neutrino mass generation and provide new particle content at the electroweak scale. We focus, mainly, on predictions and constraints set on each scenario from $\mu \rightarrow e\gamma$, $\mu \rightarrow 3e$ and $\mu - e$ conversion in the nuclei. In this class of models, the flavour structure of the Yukawa couplings between the additional scalar and fermion representations and the SM leptons is highly constrained by neutrino oscillation measurements. In particular, we show that in some regions of the parameters space of type I and type II see-saw models, the Dirac and Majorana phases of the neutrino mixing matrix, the ordering and hierarchy of the active neutrino mass spectrum as well as the value of the reactor mixing angle θ_{13} may considerably affect the size of the LFV observables. The interplay of the latter clearly allows to discriminate among the different low energy see-saw possibilities.

1 Introduction

After several decades of neutrino experiments, a clear quantitative picture of the neutrino oscillation parameters is gradually emerging (see, e.g. [1]). The Super-Kamiokande collaboration established that the atmospheric neutrino mass squared splitting is $|\Delta m_A^2| \sim \mathcal{O}(10^{-3} \text{ eV}^2)$ and that the corresponding mixing angle is large, possibly maximal $\theta_{23} \cong \pi/4$ [2]. The data from SNO, Super-Kamiokande and KamLAND experiments [3, 4, 5] allowed to establish the large mixing angle solution as a unique solution of the long standing solar neutrino problem, with a solar neutrino mass squared splitting $\Delta m_\odot^2 \sim \mathcal{O}(10^{-5} \text{ eV}^2)$

¹Also at: Institute of Nuclear Research and Nuclear Energy, Bulgarian Academy of Sciences, 1784 Sofia, Bulgaria

and mixing angle $\theta_{12} \cong \arcsin(\sqrt{0.3})$. A series of subsequent experiments, using reactor and accelerator neutrinos, have pinned down the atmospheric and solar neutrino oscillation parameters with a few to several percent accuracy, as summarized in Table 1.

Furthermore, in June of 2011 the T2K collaboration reported [6] evidence at 2.5σ for a non-zero value of the angle θ_{13} . Subsequently the MINOS [7] and Double Chooz [8] collaborations also reported evidence for $\theta_{13} \neq 0$, although with a smaller statistical significance. Global analyses of the neutrino oscillation data, including the data from the T2K and MINOS experiments, performed in [9, 10] showed that actually $\sin \theta_{13} \neq 0$ at $\geq 3\sigma$. The results of the analysis [9], in which $\Delta m_{21}^2 \equiv \Delta m_{\odot}^2$ and $|\Delta m_{31}^2| \equiv |\Delta m_{\text{A}}^2|$ were determined as well, are shown in Table 1.

Recently, the first data of the Daya Bay reactor antineutrino experiment on θ_{13} were published [11]. The value of $\sin^2 2\theta_{13}$ was measured with a rather high precision and was found to be different from zero at 5.2σ :

$$\sin^2 2\theta_{13} = 0.092 \pm 0.016 \pm 0.005, \quad 0.04 \leq \sin^2 2\theta_{13} \leq 0.14, \quad 3\sigma, \quad (1)$$

where we have given also the 3σ interval of allowed values of $\sin^2 2\theta_{13}$. Subsequently, the RENO experiment reported a 4.9σ evidence for a non-zero value of θ_{13} [12]:

$$\sin^2 2\theta_{13} = 0.113 \pm 0.013 \pm 0.019. \quad (2)$$

The value of θ_{13} determined in the RENO experiment is compatible with that measured in the Daya Bay experiment. It is interesting to note also that the mean value of $\sin^2 \theta_{13}$ found in the global analysis of the neutrino oscillation data in [9] differs very little from the mean values found in the Daya Bay and RENO experiments.

The results on θ_{13} described above will have far reaching implications for the program of research in neutrino physics. A relatively large value of $\sin \theta_{13} \sim 0.15$ opens up the possibilities, in particular, i) for searching for CP violation effects in neutrino oscillations experiments with high intensity accelerator neutrino beams (like T2K, NO ν A, etc.); ii) for determining the sign of Δm_{32}^2 , and thus the type of neutrino mass spectrum, which can be with normal or inverted ordering (see, e.g. [1]), in the long baseline neutrino oscillation experiments at accelerators (NO ν A, etc.), in the experiments studying the oscillations of atmospheric neutrinos (see, e.g. [15]), as well as in experiments with reactor antineutrinos [16]. It has important implications for the neutrinoless double beta $((\beta\beta)_{0\nu})$ decay phenomenology in the case of neutrino mass spectrum with normal ordering (NO) [17]. A value of $\sin \theta_{13} \gtrsim 0.09$ is a necessary condition for a successful “flavoured” leptogenesis when the CP violation required for the generation of the matter-antimatter asymmetry of the Universe is provided entirely by the Dirac CP violating phase in the neutrino mixing matrix [18].² As was already discussed to some extent in the literature and we will see further, in certain specific cases a value of $\sin \theta_{13} \sim 0.15$ can have important implications also for the phenomenology of the lepton flavour violation (LFV) processes involving the charged leptons in theories incorporating one of the possible TeV scale see-saw mechanisms of neutrino mass generation.

Despite the compelling evidence for the nonconservation of the leptonic flavour in neutrino oscillations, all searches for lepton flavour violation (LFV) in the charged lepton sector have

²If indeed $\sin \theta_{13} \cong 0.15$ and the neutrino mass spectrum is with inverted ordering (IO), further important implications for “flavoured” leptogenesis are possible [19].

Table 1: The best-fit values and 3σ allowed ranges of the 3-neutrino oscillation parameters, derived from a global fit of the current neutrino oscillation data, including the T2K and MINOS (but not the Daya Bay) results (from [9]). The Daya Bay data [11] on $\sin^2 \theta_{13}$ is given in the last line. The values (values in brackets) of $\sin^2 \theta_{12}$ are obtained using the “old” [13] (“new” [14]) reactor $\bar{\nu}_e$ fluxes in the analysis.

Parameter	best-fit ($\pm 1\sigma$)	3σ
Δm_{\odot}^2 [10^{-5} eV ²]	$7.58^{+0.22}_{-0.26}$	6.99 - 8.18
$ \Delta m_A^2 $ [10^{-3} eV ²]	$2.35^{+0.12}_{-0.09}$	2.06 - 2.67
$y \sin^2 \theta_{12}$	$0.306^{+0.018}_{-0.015}$	0.259(0.265) - 0.359(0.364)
$\sin^2 \theta_{23}$	$0.42^{+0.08}_{-0.03}$	0.34 - 0.64
$\sin^2 \theta_{13}$ [9]	$0.021(0.025)^{+0.007}_{-0.007}$	0.001(0.005) - 0.044(0.050)
$\sin^2 \theta_{13}$ [11]	0.0236 ± 0.0042	0.010 - 0.036

been so far negative. The best limits follow from the non-observation of the LFV muon decays $\mu^+ \rightarrow e^+ \gamma$ and $\mu^+ \rightarrow e^+ e^- e^+$,

$$\text{BR}(\mu^+ \rightarrow e^+ \gamma) < 2.4 \times 10^{-12} \quad [20], \quad (3)$$

$$\text{BR}(\mu^+ \rightarrow e^+ e^- e^+) < 1.0 \times 10^{-12} \quad [21], \quad (4)$$

and from the non-observation of conversion of muons into electrons in Titanium,

$$\text{CR}(\mu\text{Ti} \rightarrow e\text{Ti}) < 4.3 \times 10^{-12} \quad [22]. \quad (5)$$

Besides, there are stringent constraints on the tau-muon and tau-electron flavour violation from the non-observation of LFV radiative tau decays [23]:

$$\text{BR}(\tau \rightarrow \mu \gamma) < 4.4 \times 10^{-8}, \quad (6)$$

$$\text{BR}(\tau \rightarrow e \gamma) < 3.3 \times 10^{-8}. \quad (7)$$

The indicated stringent upper limits on the rates of the LFV processes involving the charged leptons lead to severe constraints on models of new physics which predict new particles at the electroweak scale coupled to the charged leptons. Indeed, the dipole operator which leads to the process $\mu \rightarrow e \gamma$ has the form:

$$-\mathcal{L} = m_\mu \bar{\mu}(f_{M1}^{\mu e} + \gamma_5 f_{E1}^{\mu e})\sigma^{\nu\rho} e F_{\nu\rho} + \text{h.c.} \quad (8)$$

where $f_{M1}^{\mu e}$ and $f_{E1}^{\mu e}$ are, respectively, the transition magnetic and electric dipole moment form factors. This operator is generated at the quantum level through particles with masses Λ which couple to the charged leptons, hence the form factors can be parameterised as $f^{\mu e} = \frac{\theta_{\mu e}^2}{16\pi^2 \Lambda^2}$, $\theta_{\mu e}$ being a parameter which measures the strength of the coupling of the new particles to the electron and the muon. The present experimental limit on $\text{BR}(\mu \rightarrow e \gamma)$ sets the following upper limit on the two form factors: $|f_{E1}^{\mu e}|, |f_{M1}^{\mu e}| \lesssim 10^{-12} \text{ GeV}^{-2}$. The latter in turn translates into $\Lambda \gtrsim 20 \text{ TeV}$ if $\theta_{\mu e} \sim 1/\sqrt{2}$, or in $\theta_{\mu e} \lesssim 0.01$ if $\Lambda \sim 300 \text{ GeV}$. It is then apparent that experiments searching for lepton flavour violation can probe models of new physics which cannot be tested in collider experiments, either because the new particles are

not kinematically accessible with the available collider energies, or because the couplings of the new particles to the Standard Model (SM) particles are too feeble to produce the former with rates necessary for their observation given the luminosity of the present colliders.

Low scale see-saw models are a particularly interesting class of models of new physics which are severely constrained by experiments searching for lepton flavour violation. In this class of models the flavour structure of the couplings of the new particles to the charged leptons is basically determined by the requirement of reproducing the data on the neutrino oscillation parameters [24, 25, 26, 27, 28]. Hence, the rates for the lepton flavour violating processes in the charged lepton sector can be calculated in terms of a few parameters, the predicted rates being possibly within the reach of the future experiments searching for lepton flavour violation, even when the parameters of the model do not allow production of the new particles with observable rates at the LHC [28].

The role of the experiments searching for lepton flavour violation to constrain low scale see-saw models will be significantly strengthened in the next years. Searches for $\mu - e$ conversion at the planned COMET experiment at KEK [29] and Mu2e experiment at Fermilab [30] aim to reach sensitivity to $\text{CR}(\mu \text{ Al} \rightarrow e \text{ Al}) \approx 10^{-16}$, while, in the longer run, the PRISM/PRIME experiment in KEK [31] and the project-X experiment in Fermilab [32] are being designed to probe values of the $\mu - e$ conversion rate on Ti, which are by 2 orders of magnitude smaller, $\text{CR}(\mu \text{ Ti} \rightarrow e \text{ Ti}) \approx 10^{-18}$ [31]. If these experiments reach the projected sensitivity without observing a signal, the upper limits on the form factors f_{M1} , f_{E1} will improve by two orders of magnitude. There are also plans to perform a new search for the $\mu^+ \rightarrow e^+ e^- e^+$ decay [33], which will probe values of the corresponding branching ratio down to $\text{BR}(\mu^+ \rightarrow e^+ e^- e^+) \approx 10^{-15}$, i.e., by 3 orders of magnitude smaller than the best current upper limit eq. (4). Furthermore, searches for tau lepton flavour violation at superB factories aim to reach a sensitivity to $\text{BR}(\tau \rightarrow (\mu, e)\gamma) \approx 10^{-9}$ [34, 35].

In this paper we will study the constraints on low (TeV) scale see-saw models of neutrino mass generation from present and future experiments searching for lepton flavour violation, with especial emphasis on $\mu - e$ conversion in nuclei, which is among all search strategies the one with brightest perspectives. The paper is organized as follows: in Sections 2, 3 and 4 we review the main features of the three types of see-saw mechanisms. We discuss for each scenario the predictions and experimental constraints on the relevant parameter space arising from LFV processes. The results are summarized and discussed in the concluding Section 5.

2 TeV Scale Type I See-Saw Model

We consider in detail in this Section LFV processes emerging in type I see-saw extensions of the SM [36]. We denote the light and heavy Majorana mass eigenstates of the type I see-saw model as χ_i and N_k , respectively.³ The charged and neutral current weak interactions involving the light Majorana neutrinos have the form:

$$\mathcal{L}_{CC}^\nu = -\frac{g}{\sqrt{2}} \bar{\ell} \gamma_\alpha \nu_{\ell L} W^\alpha + \text{h.c.} = -\frac{g}{\sqrt{2}} \bar{\ell} \gamma_\alpha ((1 + \eta)U)_{\ell i} \chi_{iL} W^\alpha + \text{h.c.}, \quad (9)$$

$$\mathcal{L}_{NC}^\nu = -\frac{g}{2c_w} \bar{\nu}_{\ell L} \gamma_\alpha \nu_{\ell L} Z^\alpha = -\frac{g}{2c_w} \bar{\chi}_{iL} \gamma_\alpha (U^\dagger(1 + \eta + \eta^\dagger)U)_{ij} \chi_{jL} Z^\alpha, \quad (10)$$

³We use the same notations as in [28, 37].

where $(1 + \eta)U = U_{\text{PMNS}}$ is the Pontecorvo, Maki, Nakagawa, Sakata (PMNS) neutrino mixing matrix [38, 39], U is a 3×3 unitary matrix which diagonalises the Majorana mass matrix of the left-handed (LH) flavour neutrinos $\nu_{\ell L}$ (generated by the see-saw mechanism), and the matrix η characterises the deviations from unitarity of the PMNS matrix. The elements of U_{PMNS} are determined in experiments studying the oscillations of the flavour neutrinos and antineutrinos, ν_{ℓ} and $\bar{\nu}_{\ell}$, $\ell = e, \mu, \tau$, at relatively low energies. In these experiments the initial states of the flavour neutrinos, produced in weak processes, are coherent superpositions of the states of the light massive Majorana neutrino χ_i only. The states of the heavy Majorana neutrino N_j are not present in the superpositions representing the initial flavour neutrino states and this leads to deviations from unitarity of the PMNS matrix.

The matrix η can be expressed in terms of a matrix RV whose elements $(RV)_{\ell k}$ determine the strength of the charged current (CC) and neutral current (NC) weak interaction couplings of the heavy Majorana neutrinos N_k to the W^{\pm} -boson and the charged lepton ℓ , and to the Z^0 boson and the left-handed (LH) flavour neutrino $\nu_{\ell L}$, $\ell = e, \mu, \tau$:

$$\mathcal{L}_{CC}^N = -\frac{g}{2\sqrt{2}} \bar{\ell} \gamma_{\alpha} (RV)_{\ell k} (1 - \gamma_5) N_k W^{\alpha} + \text{h.c.}, \quad (11)$$

$$\mathcal{L}_{NC}^N = -\frac{g}{4c_w} \bar{\nu}_{\ell L} \gamma_{\alpha} (RV)_{\ell k} (1 - \gamma_5) N_k Z^{\alpha} + \text{h.c.} \quad (12)$$

Here V is the unitary matrix which diagonalises the Majorana mass matrix of the heavy RH neutrinos and the matrix R is determined by (see [37]) $R^* \cong M_D M_N^{-1}$, M_D and M_N being the neutrino Dirac and the RH neutrino Majorana mass matrices, respectively, $|M_D| \ll |M_N|$. We have:

$$\eta \equiv -\frac{1}{2} R R^{\dagger} = -\frac{1}{2} (RV)(RV)^{\dagger} = \eta^{\dagger}. \quad (13)$$

The elements of the matrices RV and η can be constrained by using the existing neutrino oscillation data, data on electroweak (EW) processes, etc. [40, 41]. They should satisfy also the constraint which is characteristic of the type I see-saw mechanism under discussion:

$$\left| \sum_k (RV)_{\ell' k}^* M_k (RV)_{k \ell}^{\dagger} \right| \cong |(m_{\nu})_{\ell' \ell}| \lesssim 1 \text{ eV}, \quad \ell', \ell = e, \mu, \tau. \quad (14)$$

Here m_{ν} is the Majorana mass matrix of the LH flavour neutrinos generated by the see-saw mechanism. The upper limit $|(m_{\nu})_{\ell' \ell}| \lesssim 1 \text{ eV}$, $\ell, \ell' = e, \mu, \tau$, follows from the existing data on the neutrino masses and on the neutrino mixing [42]. For the values of the masses M_k of the heavy Majorana neutrinos N_k of interest for the present study, $M_k = \mathcal{O}(100 - 1000)$ GeV, the simplest scheme in which the constraint (14) can be naturally satisfied is [28] the scheme with two heavy Majorana neutrinos (see, e.g., [43, 44, 45]), N_1 and N_2 , which form a pseudo-Dirac neutrino pair [46, 47]: $M_2 = M_1(1 + z)$, where $z \ll 1$. In the scenario where the CC and NC couplings of $N_{1,2}$ are sizable, the requirement of reproducing the correct low energy neutrino oscillation parameters determines the elements $(RV)_{\ell 1}$ and $(RV)_{\ell 2}$ in eqs. (11) and (12), which take the form [28]:

$$|(RV)_{\ell 1}|^2 = \frac{1}{2} \frac{y^2 v^2}{M_1^2} \frac{m_3}{m_2 + m_3} \left| U_{\ell 3} + i \sqrt{m_2/m_3} U_{\ell 2} \right|^2, \quad \text{NH}, \quad (15)$$

$$|(RV)_{\ell 1}|^2 = \frac{1}{2} \frac{y^2 v^2}{M_1^2} \frac{m_2}{m_1 + m_2} \left| U_{\ell 2} + i \sqrt{m_1/m_2} U_{\ell 1} \right|^2 \cong \frac{1}{4} \frac{y^2 v^2}{M_1^2} |U_{\ell 2} + i U_{\ell 1}|^2, \quad \text{IH}, \quad (16)$$

where y represents the maximum eigenvalue of the neutrino Yukawa matrix and $v \simeq 174$ GeV. In the last equation we have used the fact that for the IH spectrum one has $m_1 \cong m_2$. These expressions obey the relation [28]:

$$(RV)_{\ell 2} = \pm i (RV)_{\ell 1} \sqrt{\frac{M_1}{M_2}}, \quad \ell = e, \mu, \tau. \quad (17)$$

and thus eq. (14) is automatically satisfied.

Upper bounds on the couplings of RH neutrinos with SM particles can be obtained from the low energy electroweak precision data on lepton number conserving processes like $\pi \rightarrow \ell \bar{\nu}_\ell$, $Z \rightarrow \nu \bar{\nu}$ and other tree-level processes involving light neutrinos in the final state [40]. These bounds read:

$$|(RV)_{e1}|^2 \lesssim 2 \times 10^{-3}, \quad (18)$$

$$|(RV)_{\mu 1}|^2 \lesssim 0.8 \times 10^{-3}, \quad (19)$$

$$|(RV)_{\tau 1}|^2 \lesssim 2.6 \times 10^{-3}. \quad (20)$$

Let us add that in the class of type I see-saw models with two heavy Majorana neutrinos we are considering (see, e.g., [43, 44, 45]), one of the three light (Majorana) neutrinos is massless and hence the neutrino mass spectrum is hierarchical. Two possible types of hierarchical spectrum are allowed by the current neutrino data (see, e.g., [1]): *i*) normal hierarchical (NH), $m_1 = 0$, $m_2 = \sqrt{\Delta m_\odot^2}$ and $m_3 = \sqrt{\Delta m_A^2}$, where $\Delta m_\odot^2 \equiv m_2^2 - m_1^2 > 0$ and $\Delta m_A^2 \equiv m_3^2 - m_1^2$; *ii*) inverted hierarchical (IH), $m_3 = 0$, $m_2 = \sqrt{|\Delta m_A^2|}$ and $m_1 = \sqrt{|\Delta m_A^2| - \Delta m_\odot^2} \cong \sqrt{|\Delta m_A^2|}$, where $\Delta m_\odot^2 \equiv m_2^2 - m_1^2 > 0$ and $\Delta m_A^2 \equiv m_3^2 - m_2^2 < 0$. In both cases we have: $\Delta m_\odot^2 / |\Delta m_A^2| \cong 0.03 \ll 1$.

The numerical results we will present further will be obtained employing the standard parametrisation for the unitary matrix U :

$$U = V(\theta_{12}, \theta_{23}, \theta_{13}, \delta) Q(\alpha_{21}, \alpha_{31}). \quad (21)$$

Here (see, e.g., [1])

$$V = \begin{pmatrix} 1 & 0 & 0 \\ 0 & c_{23} & s_{23} \\ 0 & -s_{23} & c_{23} \end{pmatrix} \begin{pmatrix} c_{13} & 0 & s_{13}e^{-i\delta} \\ 0 & 1 & 0 \\ -s_{13}e^{i\delta} & 0 & c_{13} \end{pmatrix} \begin{pmatrix} c_{12} & s_{12} & 0 \\ -s_{12} & c_{12} & 0 \\ 0 & 0 & 1 \end{pmatrix}, \quad (22)$$

where we have used the standard notation $c_{ij} \equiv \cos \theta_{ij}$, $s_{ij} \equiv \sin \theta_{ij}$, δ is the Dirac CP violation (CPV) phase and the matrix Q contains the two Majorana CPV phases ⁴ [48],

$$Q = \text{diag}(1, e^{i\alpha_{21}/2}, e^{i\alpha_{31}/2}). \quad (23)$$

We recall that $U_{\text{PMNS}} = (1 + \eta)U$. Thus, up to corrections which depend on the elements of the matrix η whose absolute values, however, do not exceed approximately 5×10^{-3} [40], the values of the angles θ_{12} , θ_{23} and θ_{13} coincide with the values of the solar neutrino,

⁴ In the case of the type II see-saw mechanism, to be discussed in Section 3, we have $\eta = 0$ and thus the neutrino mixing matrix coincides with U : $U_{\text{PMNS}} = U$. We will employ the parametrisation (21) - (23) for U also in that case.

atmospheric neutrino and the 1-3 (or “reactor”) mixing angles, determined in the 3-neutrino mixing analyses of the neutrino oscillation data and reported in Table 1.

Given the neutrino masses and mixing angles, the TeV scale type I see-saw scenario we are considering is characterised by four parameters [28]: the mass (scale) M_1 , the Yukawa coupling y , the parameter z of the splitting between the masses of the two heavy Majorana neutrinos and a phase ω . The mass M_1 and the Yukawa coupling y can be determined, in principle, from the measured rates of two lepton flavour violating (LFV) processes, the $\mu \rightarrow e\gamma$ decay and the $\mu - e$ conversion in nuclei, for instance. The mass splitting parameter z and the phase ω , together with M_1 and y , enter, e.g., into the expression for the rate of $(\beta\beta)_{0\nu}$ -decay, predicted by the model. The latter was discussed in detail in [28].

2.1 The $\mu \rightarrow e\gamma$ Decay

In this subsection we update briefly the discussion of the limits on the parameters of the TeV scale type I see-saw model, derived in [28] using the experimental upper bound on the $\mu \rightarrow e\gamma$ decay rate obtained in 1999 in the MEGA experiment [49]. After the publication of [28], the MEG collaboration reported a new more stringent upper bound on the $\mu \rightarrow e\gamma$ decay rate [20] given in eq. (3). Such an update is also necessary in view of the relatively large nonzero value of the reactor angle θ_{13} measured in the Daya Bay and RENO experiments [11, 12] and reported in eqs. (1) and (2). As was discussed in [28], in particular, the rate of the $\mu \rightarrow e\gamma$ decay in the type I see-saw scheme considered can be strongly suppressed for certain values of θ_{13} .

The $\mu \rightarrow e\gamma$ decay branching ratio in the scenario under discussion is given by [50, 51]:

$$\text{BR}(\mu \rightarrow e\gamma) = \frac{\Gamma(\mu \rightarrow e\gamma)}{\Gamma(\mu \rightarrow e + \nu_\mu + \bar{\nu}_e)} = \frac{3\alpha_{\text{em}}}{32\pi} |T|^2, \quad (24)$$

where α_{em} is the fine structure constant and [28]

$$|T| \cong \frac{2+z}{1+z} |(RV)_{\mu 1}^* (RV)_{e 1}| |G(X) - G(0)|. \quad (25)$$

In eqs. (24) and (25) the loop integration function $G(x)$ has the form:

$$G(x) = \frac{10 - 43x + 78x^2 - 49x^3 + 4x^4 + 18x^3 \log(x)}{3(x-1)^4}, \quad (26)$$

where $X \equiv (M_1/M_W)^2$. In deriving the expression for the matrix element T , eq. (25), we have assumed that the difference between M_1 and M_2 is negligibly small and used $M_1 \cong M_2$. It is easy to verify that $G(x)$ is a monotonic function which takes values in the interval $[4/3, 10/3]$, with $G(x) \cong \frac{10}{3} - x$ for $x \ll 1$.

Using the expressions of $|(RV)_{\mu 1}|^2$ and $|(RV)_{e 1}|^2$ in terms of neutrino parameters, eqs. (15)

and (16), we obtain the $\mu \rightarrow e\gamma$ decay branching ratio for the NH and IH spectra:

$$\text{NH : } \text{BR}(\mu \rightarrow e\gamma) \cong \frac{3\alpha_{\text{em}}}{32\pi} \left(\frac{y^2 v^2}{M_1^2} \frac{m_3}{m_2 + m_3} \right)^2 \left| U_{\mu 3} + i\sqrt{\frac{m_2}{m_3}} U_{\mu 2} \right|^2 \left| U_{e 3} + i\sqrt{\frac{m_2}{m_3}} U_{e 2} \right|^2 [G(X) - G(0)]^2, \quad (27)$$

$$\text{IH : } \text{BR}(\mu \rightarrow e\gamma) \cong \frac{3\alpha_{\text{em}}}{32\pi} \left(\frac{y^2 v^2}{M_1^2} \frac{1}{2} \right)^2 |U_{\mu 2} + iU_{\mu 1}|^2 |U_{e 2} + iU_{e 1}|^2 [G(X) - G(0)]^2. \quad (28)$$

The data on the process $\mu \rightarrow e\gamma$ set very stringent constraints on the TeV scale type I see-saw mechanism. The current upper bound on $\text{BR}(\mu \rightarrow e\gamma)$ was obtained in the MEG experiment at PSI [20] and is given in eq. (3). It is an improvement by a factor of 5 of the previous best upper limit of the MEGA experiment, published in 1999 [49]. The projected sensitivity of the MEG experiment is $\text{BR}(\mu \rightarrow e\gamma) \sim 10^{-13}$ [20]. For $M_1 = 100$ GeV ($M_1 = 1$ TeV) and $z \ll 1$ we get the following upper limit on the product $|(RV)_{\mu 1}^* (RV)_{e 1}|$ of the heavy Majorana neutrino couplings to the muon (electron) and the W^\pm boson and to the Z^0 boson from the the upper limit eq. (3):

$$|(RV)_{\mu 1}^* (RV)_{e 1}| < 0.8 \times 10^{-4} (0.3 \times 10^{-4}), \quad (29)$$

where we have used eqs. (24) and (25). This can be recast as an upper bound on the neutrino Yukawa coupling y . Taking, *e.g.*, the best fit values of the solar and atmospheric oscillation parameters given in Table 1, we get:

$$y \lesssim 0.035 \text{ (0.21) for NH with } M_1 = 100 \text{ GeV (1000 GeV) and } \sin \theta_{13} = 0.1, \quad (30)$$

$$y \lesssim 0.025 \text{ (0.15) for IH with } M_1 = 100 \text{ GeV (1000 GeV) and } \sin \theta_{13} = 0.1. \quad (31)$$

The constraints which follow from the current MEG upper bound on $\text{BR}(\mu \rightarrow e\gamma)$ will not be valid in the case of a cancellation between the different terms in one of the factors $|U_{\ell 3} + i\sqrt{m_2/m_3} U_{\ell 2}|^2$ and $|U_{\ell 2} + iU_{\ell 1}|^2$, $\ell = e, \mu$, in the expressions (27) and (28) for $\text{BR}(\mu \rightarrow e\gamma)$. Employing the standard parametrisation of U , eqs. (21) - (23), one can show that in the case of NH spectrum we can have $|U_{e 3} + i\sqrt{m_2/m_3} U_{e 2}| = 0$ if [28] (see also [24]) $\sin(\delta + (\alpha_{21} - \alpha_{31})/2) = 1$ and $\tan \theta_{13} = (\Delta m_\odot^2 / \Delta m_\text{A}^2)^{1/4} \sin \theta_{12}$. Using the 3σ allowed ranges of Δm_\odot^2 , Δm_A^2 and $\sin^2 \theta_{12}$ given in Table 1, we find that the second condition can be satisfied provided $\sin^2 \theta_{13} \gtrsim 0.04$, which lies outside the 3σ range of allowed values of $\sin^2 \theta_{13}$ found in the Daya Bay experiment [11] (see eq. (1)).

In the case of IH spectrum, the factor $|U_{e 2} + iU_{e 1}|^2$ can be rather small for $\sin(\alpha_{21}/2) = -1$: $|U_{e 2} + iU_{e 1}|^2 = c_{13}^2 (1 - \sin 2\theta_{12}) \cong 0.0765$, where we have used the best fit values of $\sin^2 \theta_{12} = 0.306$ and $\sin^2 \theta_{13} = 0.0236$. It is also possible to have a strong suppression of the factor $|U_{\mu 2} + iU_{\mu 1}|^2$ [28]. Indeed, using the standard parametrisation of the matrix U it is not difficult to show that for fixed values of the angles θ_{12} , θ_{23} and of the phases α_{21} and δ , $|U_{\mu 2} + iU_{\mu 1}|^2$ has a minimum for

$$\sin \theta_{13} = \frac{c_{23}}{s_{23}} \frac{\cos 2\theta_{12} \cos \delta \sin \frac{\alpha_{21}}{2} - \cos \frac{\alpha_{21}}{2} \sin \delta}{1 + 2c_{12} s_{12} \sin \frac{\alpha_{21}}{2}}. \quad (32)$$

At the minimum we get:

$$\min(|U_{\mu 2} + iU_{\mu 1}|^2) = c_{23}^2 \frac{(\cos \delta \cos \frac{\alpha_{21}}{2} + \cos 2\theta_{12} \sin \delta \sin \frac{\alpha_{21}}{2})^2}{1 + 2c_{12} s_{12} \sin \frac{\alpha_{21}}{2}}. \quad (33)$$

Notice that, from the equation above, the $\mu \rightarrow e\gamma$ branching ratio is highly suppressed if the Dirac and Majorana phases take CP conserving values, mainly: $\delta \simeq 0$ and $\alpha_{21} \simeq \pi$. In this case, from eq. (32) we get the lower bound $\sin(\theta_{13}) \gtrsim 0.13$, which is in agreement with the Daya Bay measurement reported in Tab. 1. On the other hand, assuming CPV phases, we still may have $\min(|U_{\mu 2} + iU_{\mu 1}|^2) = 0$, provided θ_{12} and the Dirac and Majorana phases δ and α_{21} satisfy the following conditions: $\cos \delta \cos(\alpha_{21}/2) + \cos 2\theta_{12} \sin \delta \sin(\alpha_{21}/2) = 0$ and $\text{sgn}(\cos \delta \cos \frac{\alpha_{21}}{2}) = -\text{sgn}(\sin \delta \sin \frac{\alpha_{21}}{2})$. Taking $\cos \delta > 0$ ($\cos \delta < 0$) and using $\tan \delta = -\tan(\alpha_{21}/2)/\cos 2\theta_{12}$ in eq. (32), we get the relation between s_{13} , δ and $\cos 2\theta_{12}$, for which $\min(|U_{\mu 2} + iU_{\mu 1}|^2) = 0$:

$$\sin \theta_{13} = \frac{c_{23}}{s_{23}} \frac{\sqrt{1 + \tan^2 \delta} \cos 2\theta_{12}}{\sqrt{1 + \cos^2 2\theta_{12} \tan^2 \delta} + 2c_{12} s_{12} \text{sgn}(\cos \delta)}. \quad (34)$$

Using the 3σ intervals of allowed values of $\sin^2 \theta_{12}$ and $\sin^2 \theta_{23}$ (found with the “new” reactor $\bar{\nu}_e$ fluxes, see Table 1) and allowing δ to vary in the interval $[0, 2\pi]$, we find that the values of $\sin \theta_{13}$ obtained using eq. (34) lie in the interval $\sin \theta_{13} \gtrsim 0.11$. As it follows from eq. (1), we have at 3σ : $0.10 \lesssim \sin \theta_{13} \lesssim 0.19$. The values of $0.11 \lesssim \sin \theta_{13} \lesssim 0.19$ correspond to $0 \leq \delta \lesssim 0.7$. These conclusions are illustrated in Fig. 1. For $\sin \theta_{13}$ and δ lying in the indicated intervals we can have $|U_{\mu 2} + iU_{\mu 1}|^2 = 0$ and thus a strong suppression of the $\mu \rightarrow e\gamma$ decay rate. As we will see in subsections 2.2 and 2.3, in the model we are considering, the predicted $\mu - e$ conversion rate in a given nucleus and $\mu \rightarrow 3e$ decay rate are also proportional to $|(RV)_{\mu 1}^* (RV)_{e 1}|^2$, as like the $\mu \rightarrow e\gamma$ decay rate. This implies that in the case of the TeV scale type I see-saw mechanism and IH light neutrino mass spectrum, if, e.g., $\text{BR}(\mu \rightarrow e\gamma)$ is strongly suppressed due to $|U_{\mu 2} + iU_{\mu 1}|^2 \cong 0$, the $\mu - e$ conversion and the $\mu \rightarrow 3e$ decay rates will also be strongly suppressed⁵. The suppression under discussion cannot hold if, for instance, it is experimentally established that δ is definitely bigger than 1.0. That would be the case if the existing indications [9] that $\cos \delta < 0$ receive unambiguous confirmation.

The limits on the parameters $|(RV)_{\mu 1}|$ and $|(RV)_{e 1}|$, implied by the electroweak precision data, eqs. (18) - (20), and the upper bound on $\text{BR}(\mu \rightarrow e\gamma)$, eq. (3), are illustrated in Fig. 2. The results shown are obtained for the best fit values of $\sin \theta_{13} = 0.156$ and of the other neutrino oscillation parameters given in Table 1.

2.2 The $\mu - e$ Conversion in Nuclei

We will discuss next the predictions of the TeV scale type I see-saw extension of the SM for the rate of the $\mu - e$ conversion in nuclei, as well as the experimental constraints that can

⁵ Let us note that in the case of IH spectrum we are discussing actually one has $|(RV)_{\mu 1}|^2 \propto |U_{\mu 2} + i\sqrt{m_1/m_2}U_{\mu 1}|^2$ (see eq. (16)), with $m_2 = \sqrt{|\Delta m_A^2|}$ and $m_1 = \sqrt{|\Delta m_A^2| - \Delta m_\odot^2} \cong \sqrt{|\Delta m_A^2|}(1 - 0.5\Delta m_\odot^2/|\Delta m_A^2|)$. Therefore when $|U_{\mu 2} + iU_{\mu 1}| = 0$ we still have $|U_{\mu 2} + i\sqrt{m_1/m_2}U_{\mu 1}|^2 \neq 0$. However, in this case $|U_{\mu 2} + i\sqrt{m_1/m_2}U_{\mu 1}|^2 \cong (\Delta m_\odot^2/(4|\Delta m_A^2|))^2 |U_{\mu 1}|^2 \lesssim 1.7 \times 10^{-5}$, where we have used $\delta = 0$ (which maximises $|U_{\mu 1}|^2$) and the best fit values of the other neutrino oscillation parameters. Thus, our conclusions about the suppression of $\text{BR}(\mu \rightarrow e\gamma)$, the $\mu - e$ conversion and the $\mu \rightarrow 3e$ decay rates are still valid.

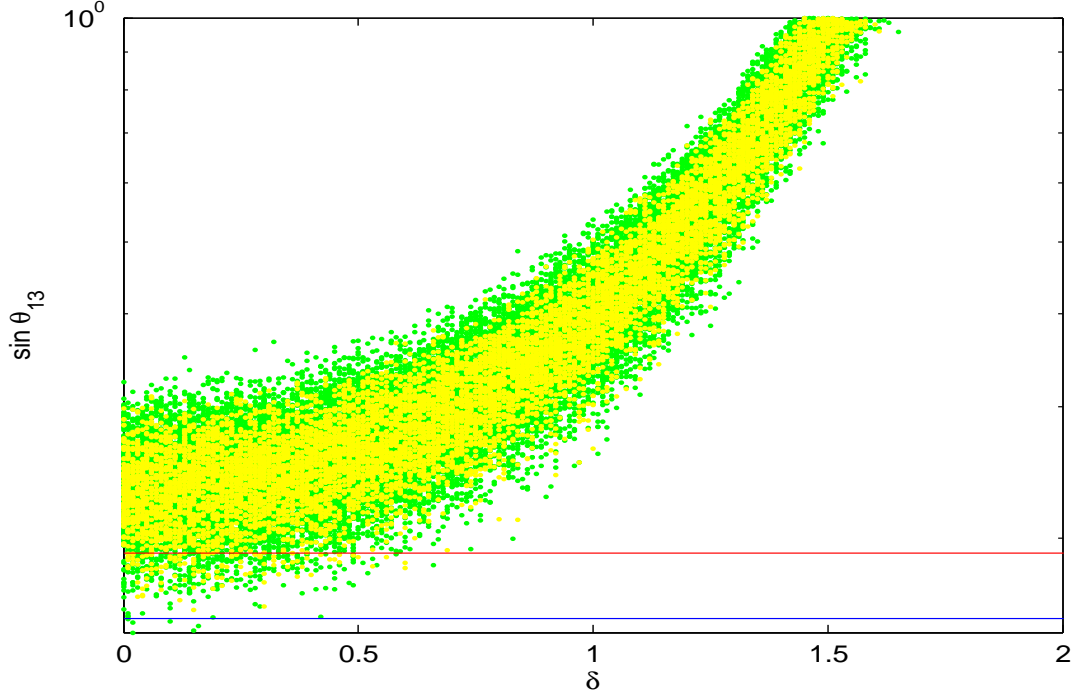


Figure 1: Values of $\sin \theta_{13}$, as a function of the phase δ , which yield a suppressed rate of the process $\mu \rightarrow e\gamma$. The values are obtained using eq. (34), the 2σ (3σ) intervals of allowed values of $\sin^2 \theta_{12}$ and $\sin^2 \theta_{23}$, yellow (green) points (found with the “new” reactor $\bar{\nu}_e$ fluxes, see Table 1) and allowing δ to vary in the interval $[0, 2\pi]$. The red and blue horizontal lines correspond to the 3σ upper limit $\sin \theta_{13} = 0.191$ and the best fit value $\sin \theta_{13} = 0.156$.

be imposed on this see-saw scenario by the current and prospective $\mu - e$ conversion data. In the type I see-saw scenario of interest, the $\mu - e$ conversion rate in a nucleus \mathcal{N} is very well approximated by the expression [52]:

$$\text{CR}(\mu \mathcal{N} \rightarrow e \mathcal{N}) \equiv \frac{\Gamma(\mu \mathcal{N} \rightarrow e \mathcal{N})}{\Gamma_{\text{capt}}} = \frac{\alpha_{\text{em}}^5}{2\pi^4} \frac{Z_{\text{eff}}^4}{Z} |F(-m_\mu^2)|^2 \frac{G_F^2 m_\mu^5}{\Gamma_{\text{capt}}} |(RV)_{\mu 1}^* (RV)_{e 1}|^2 |\mathcal{C}_{\mu e}|^2. \quad (35)$$

In eq. (35) Z and N are the proton number and the neutron number of the nucleus \mathcal{N} , respectively, $F(-m_\mu^2)$ is the nuclear form factor at momentum transfer squared $q^2 = -m_\mu^2$, m_μ being the muon mass, Z_{eff} is an effective atomic charge and Γ_{capt} is the experimentally known total muon capture rate. The loop integral factor $\mathcal{C}_{\mu e}$ receives contributions from γ -penguin, Z^0 -penguin and box type diagrams and reads [52]:

$$\mathcal{C}_{\mu e} \cong \left[Z (4R_0(X) + H'_0(X)) - (2Z + N) \frac{X_0(X)}{\sin^2 \theta_W} + (Z + 2N) \frac{Y_0(X)}{\sin^2 \theta_W} \right]. \quad (36)$$

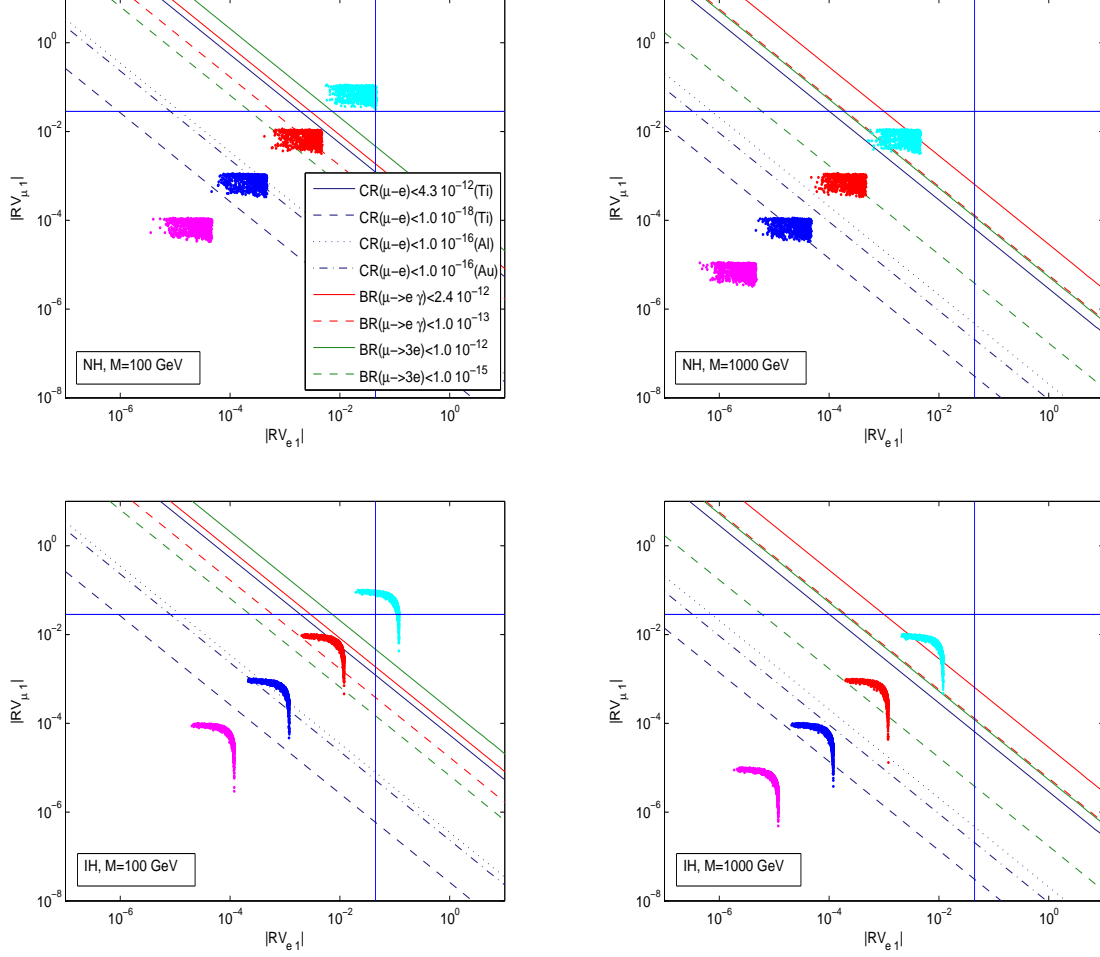


Figure 2: Correlation between $|(RV)_{e1}|$ and $|(RV)_{\mu 1}|$ in the case of NH (upper panels) and IH (lower panels) light neutrino mass spectrum, for $M_1 = 100$ (1000) GeV and, *i*) $y = 0.0001$ (magenta points), *ii*) $y = 0.001$ (blue points), *iii*) $y = 0.01$ (red points) and *iv*) $y = 0.1$ (cyan points). The constraints from several LFV processes discussed in the text are shown.

Here θ_W is the weak mixing angle, $\sin^2 \theta_W = 0.23$, Z and N are the proton and neutron numbers of the nucleus \mathcal{N} , $X = M_1^2/M_W^2$, and

$$R_0(y) = \frac{y(6y^3 - 55y^2 + 79y - 24)}{48(y-1)^3} + \frac{y(8y^3 - 2y^2 - 15y + 6)}{24(y-1)^4} \log y, \quad (37)$$

$$H'_0(y) = \frac{y(2y^2 + 5y - 1)}{4(y-1)^3} - \frac{3y^3 \log y}{2(y-1)^4}, \quad (38)$$

$$X_0(y) = \frac{y}{8} \left[\frac{y+2}{y-1} + \frac{3y-6}{(y-1)^2} \ln y \right], \quad (39)$$

$$Y_0(y) = \frac{y}{8} \left[\frac{y-4}{y-1} + \frac{3y}{(y-1)^2} \ln y \right]. \quad (40)$$

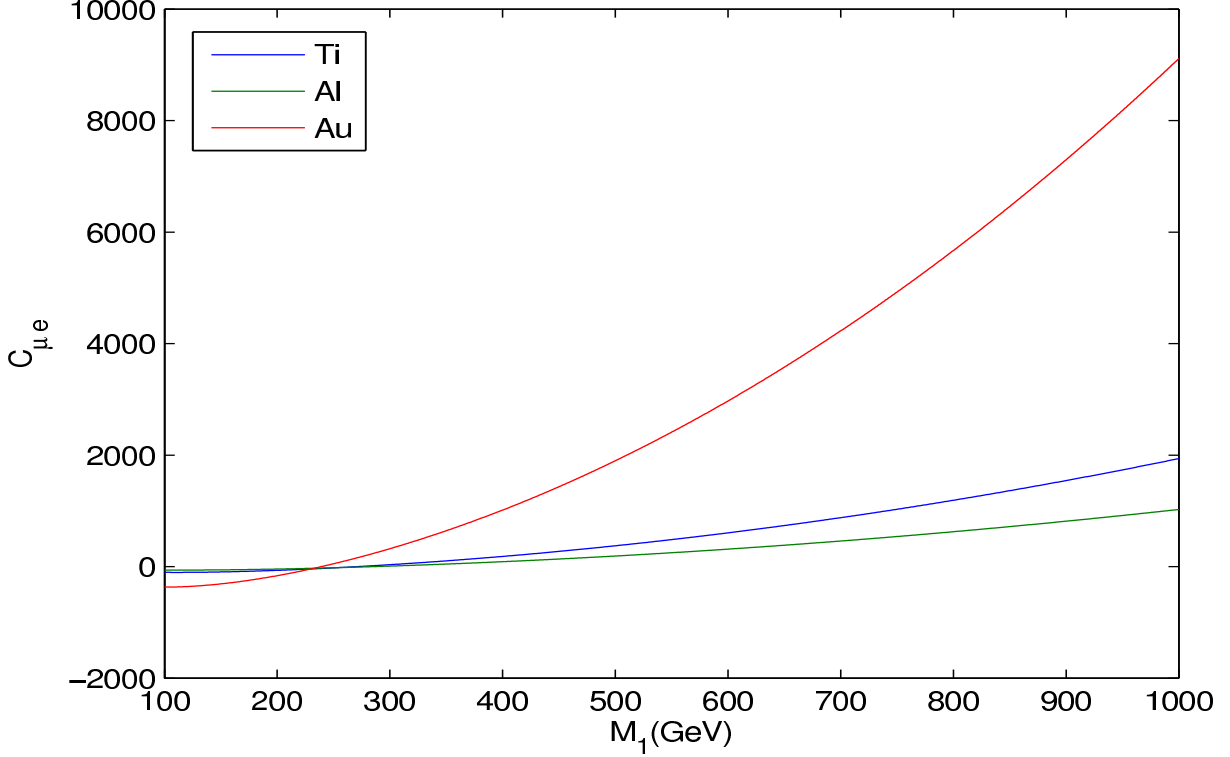


Figure 3: The $\mu - e$ conversion loop integration factor $C_{\mu e}$ versus the see-saw mass scale M_1 , for three different nuclei: i) $^{48}_{22}\text{Ti}$ (blue line), ii) $^{27}_{13}\text{Al}$ (green line), and iii) $^{197}_{79}\text{Au}$ (red line).

In what follows we will present results for three nuclei which were used in the past, and are of interest for possible future $\mu - e$ conversion experiments: $^{48}_{22}\text{Ti}$, $^{27}_{13}\text{Al}$ and $^{197}_{79}\text{Au}$. For these nuclei one has, respectively: i) $Z_{eff} = 17.6$; 11.62 ; 33.64 , ii) $F(q^2 = -m_\mu^2) \approx 0.54$; 0.64 ; 0.20 , and iii) $\Gamma_{\text{capt}} = 2.59$; 0.69 ; $13.07 \times 10^6 \text{ sec}^{-1}$ [31].

The dependence of the loop integration factor $C_{\mu e}$ on the see-saw mass scale M_1 for the three nuclei of interest is shown in Fig. 3. The first feature to notice is that $C_{\mu e}$ for $^{48}_{22}\text{Ti}$, $^{27}_{13}\text{Al}$ and $^{197}_{79}\text{Au}$ goes through zero at $M_1 = 271$; 285 ; 239 GeV, respectively. At $M_1 = 271$ GeV, $|C_{\mu e}|$ for $^{27}_{13}\text{Al}$ and $^{197}_{79}\text{Au}$ takes the values $|C_{\mu e}(\text{Al})| \cong 8.6$ and $|C_{\mu e}(\text{Au})| \cong 158.0$; at $M_1 = 285$ GeV, we have $|C_{\mu e}(\text{Ti})| \cong 16.2$ and $|C_{\mu e}(\text{Au})| \cong 234.5$; and finally, at $M_1 = 239$ GeV, we find $|C_{\mu e}(\text{Ti})| \cong 33.4$ and $|C_{\mu e}(\text{Al})| \cong 26.3$. Thus, for the values of M_1 at which $C_{\mu e}(\text{Ti}) = 0$ or $C_{\mu e}(\text{Al}) = 0$, $|C_{\mu e}(\text{Au})|$ has a rather large value, while at the value at which $C_{\mu e}(\text{Au}) = 0$, $|C_{\mu e}(\text{Ti})|$ and $|C_{\mu e}(\text{Al})|$ are not strongly suppressed.

The interval where, e.g., $|C_{\mu e}| \leq 1$ (10) in the case of $\mu - e$ conversion on Ti reads: 270 (262) GeV $\lesssim |C_{\mu e}| \lesssim 272$ (280) GeV. For a conversion on Al or Au these intervals are 284 (269) GeV $\lesssim |C_{\mu e}| \lesssim 269$ (301) GeV and 239.0 (237) GeV $\lesssim |C_{\mu e}| \lesssim 239.4$ (241) GeV, respectively.

For M_1 lying outside these relatively narrow intervals centered on the values of M_1 at which $C_{\mu e} = 0$, $|C_{\mu e}|$ takes rather large values for each of the three nuclei. For $M = 100$ GeV, for instance, we find $|C_{\mu e}(\text{Ti})| \cong 102$, $|C_{\mu e}(\text{Al})| \cong 61$ and $|C_{\mu e}(\text{Au})| \cong 367$; for $M = 1000$ GeV one has: $|C_{\mu e}(\text{Ti})| \cong 1936$, $|C_{\mu e}(\text{Al})| \cong 1024$ and $|C_{\mu e}(\text{Au})| \cong 9110$.

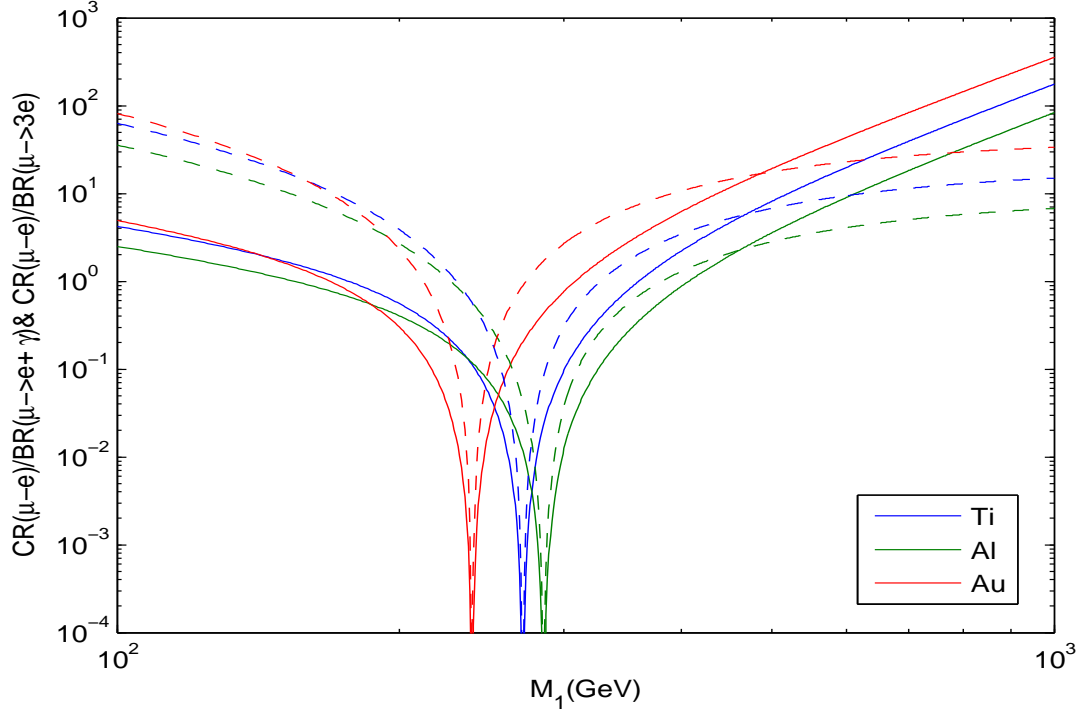


Figure 4: The ratio of the $\mu - e$ relative conversion rate and the branching ratio of the i) $\mu \rightarrow e\gamma$ decay (solid lines), ii) $\mu \rightarrow 3e$ decay (dashed lines), versus the type I see-saw mass scale M_1 , for three different nuclei: $^{48}_{22}\text{Ti}$ (blue lines), $^{27}_{13}\text{Al}$ (green lines) and $^{197}_{79}\text{Au}$ (red lines).

It follows from these considerations that the $\mu - e$ conversion rate on, e.g., Ti, is strongly enhanced by the value of the loop integration factor $|\mathcal{C}_{\mu e}|$ for $M_1 \cong (100 - 250)$ GeV and for $M_1 \gtrsim 300$ GeV. Similar results hold for the $\mu - e$ conversion rate on Al and Au nuclei. At $M_1 = 1000$ GeV, for instance, the corresponding enhancement factors are $\sim 10^6$ for the Ti and Al nuclei ⁶, while for the Au nucleus it is $\sim 10^7$. As a consequence, the rate of $\mu - e$ conversion has a remarkable sensitivity to the product $|(RV)_{\mu 1}^*(RV)_{e 1}|$ of CC couplings of the heavy Majorana neutrinos to the electron and muon for most of the values of M_1 from the interval of interest (100 – 1000) GeV, the only exception being the narrow intervals of values of M_1 , quoted above, for which the conversion rate is suppressed.

The best experimental upper bound on the conversion rate is [22]: $\text{CR}(\mu \text{ Ti} \rightarrow e \text{ Ti}) \lesssim 4.3 \times 10^{-12}$. This bound implies a constraint on $|(RV)_{\mu 1}^*(RV)_{e 1}|$, which is shown in Fig. 2 for $M_1 = 100; 1000$ GeV. It is quite remarkable that, as Fig. 2 shows, the constraint on the product of couplings $|(RV)_{\mu 1}^*(RV)_{e 1}|$ implied by the best experimental upper limit on $\text{CR}(\mu \text{ Ti} \rightarrow e \text{ Ti})$ is more stringent than the constraint following from the best experimental upper limit on $\text{BR}(\mu \rightarrow e\gamma)$ although the two experimental upper limits are very similar quantitatively and the expression for $\text{CR}(\mu \text{ Ti} \rightarrow e \text{ Ti})$ has an additional factor of $\alpha = 1/137$ with respect to the expression for $\text{BR}(\mu \rightarrow e\gamma)$.

⁶Note that although $|\mathcal{C}_{\mu e}|^2$ increases monotonically with the increase of $M_1 \gtrsim 300$ GeV, the factor $|(RV)_{\mu 1}^*(RV)_{e 1}|^2$ in the expression for the conversion rate $\text{CR}(\mu \mathcal{N} \rightarrow e \mathcal{N})$ decreases as M_1^4 , so that $\text{CR}(\mu \mathcal{N} \rightarrow e \mathcal{N})$ has a finite limit when M_1 tends to infinity.

Future experimental searches for $\mu - e$ conversion in $^{48}_{22}\text{Ti}$ can reach the sensitivity of $\text{CR}(\mu \text{ Ti} \rightarrow e \text{ Ti}) \approx 10^{-18}$ [31]. Therefore, for values of M_1 outside the narrow intervals quoted above for which the loop integration factor $|\mathcal{C}_{\mu e}|$ is strongly suppressed, an upper bound on the $\mu - e$ conversion ratio of $\mathcal{O}(10^{-18})$ can be translated into the following stringent constraint on the heavy Majorana neutrino CC couplings to the muon and electron:

$$|(RV)^*_{\mu 1}(RV)_{e 1}| \lesssim 2.6 \times 10^{-8} \quad (0.14 \times 10^{-8}) \quad \text{for } M_1 \approx 100 \text{ (1000) GeV}. \quad (41)$$

As was noticed earlier, the two parameters of the type I see-saw model considered, the mass scale M_1 and the Yukawa coupling y , can be determined, in principle, from data on $\text{BR}(\mu \rightarrow e\gamma)$ (or $\text{BR}(\mu \rightarrow 3e)$) and $\text{CR}(\mu \text{ Ti} \rightarrow e \text{ Ti})$ if the two processes will be observed. Actually, the ratio of the rates of $\mu - e$ conversion in any given nucleus \mathcal{N} , $\text{CR}(\mu \mathcal{N} \rightarrow e \mathcal{N})$, and of the $\mu \rightarrow e\gamma$ decay, depends only on the mass (scale) M_1 and can be used, in principle, to determine the latter. In the case of $\mu - e$ conversion on titanium, for instance, we find:

$$R\left(\frac{\mu - e}{\mu \rightarrow e\gamma}\right) \equiv \frac{\text{CR}(\mu \text{ Ti} \rightarrow e \text{ Ti})}{\text{BR}(\mu \rightarrow e\gamma)} \approx 4.2 \text{ (174)} \quad \text{for } M_1 \approx 100 \text{ (1000) GeV}. \quad (42)$$

The correlation between $\text{CR}(\mu \mathcal{N} \rightarrow e \mathcal{N})$ and $\text{BR}(\mu \rightarrow e\gamma)$ in the model considered is illustrated in Fig. 4. As Fig. 4 indicates, a measured value of $R(\frac{\mu - e}{\mu \rightarrow e\gamma}) \lesssim 5$ would be compatible with two values of M_1 .

The type I see-saw mass scale M_1 would be uniquely determined if $\mu - e$ conversion is observed in two different nuclei or if, e.g., the $\mu \rightarrow e\gamma$ decay or $\mu - e$ conversion in a given nucleus is observed and it is experimentally established that $R(\frac{\mu - e}{\mu \rightarrow e\gamma}) \lesssim 10^{-3}$. In the latter case M_1 could be determined with a relatively high precision. Furthermore, if one restricts to RH neutrino masses in the range (50 – 1000) GeV, the mass scale M_1 would also be uniquely determined if it is found that $R(\frac{\mu - e}{\mu \rightarrow e\gamma}) > 20$.

We note also that the correlation between $\text{CR}(\mu \mathcal{N} \rightarrow e \mathcal{N})$ and $\text{BR}(\mu \rightarrow e\gamma)$ in the type I see-saw model considered is qualitatively and quantitatively very different from the correlation in models where the $\mu - e$ conversion is dominated by the photon penguin diagram, e.g., the supersymmetric high-scale see-saw model which predicts approximately [54] $\text{CR}(\mu \text{ Ti} \rightarrow e \text{ Ti}) \approx 5 \times 10^{-3} \text{BR}(\mu \rightarrow e\gamma)$.

2.3 The $\mu \rightarrow 3e$ decay

The $\mu \rightarrow 3e$ decay branching ratio has been calculated in [52] in a supersymmetric scenario with lepton flavour violation. Adapting their results to the case we are interested in we get:

$$\text{BR}(\mu \rightarrow 3e) = \frac{4\alpha_{em}^2}{\pi^2} |(RV)^*_{\mu 1}(RV)_{e 1}|^2 |C_{\mu 3e}(M_1^2/M_W^2)|^2, \quad (43)$$

$$\begin{aligned} |C_{\mu 3e}(y)|^2 &= 3\bar{Z}^2(y) + 3\bar{Z}(y)H(y) + H^2(y) \left(\log \frac{m_\mu}{m_e} - \frac{11}{8} \right) \\ &+ \frac{1}{2\sin^4\theta_W} \bar{Y}_e^2 - \frac{2}{\sin^2\theta_W} \bar{Z}\bar{Y}_e - \frac{1}{\sin^2\theta_W} H(y)\bar{Y}_e. \end{aligned} \quad (44)$$

Here $H(y)$ and $\bar{Z}(y)$ correspond to the dipole and charged radius type operators originating from the photon penguin diagram of the decay, while $\bar{Y}_e(y)$ corresponds to the box diagram

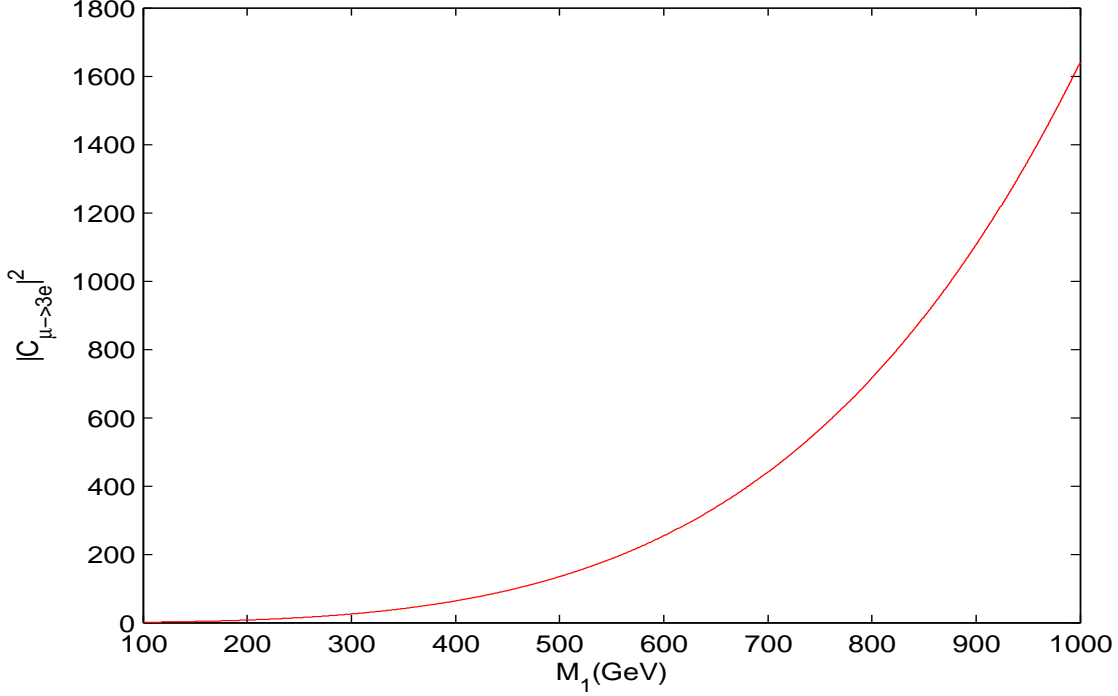


Figure 5: The $\mu \rightarrow 3e$ decay rate factor $|C_{\mu 3e}|^2$ as a function of the see-saw mass scale M_1 .

contribution. We have: $H(y) = (G(y) - G(0))/4$, $\bar{Y}_e(y) = Y_0(y) - |(RV)_{e1}|^2 S_0(y) \approx Y_0(y)$, where $G(y)$ and $Y_0(y)$ are given in eqs. (26) and (40), respectively, and $\bar{Z}(y) = C_0(y) + (D_0(y) - 2E_0(y)/3)/4$ with

$$C_0(y) = \frac{y}{8} \left[\frac{y-6}{y-1} + \frac{3y+2}{(y-1)^2} \log y \right], \quad (45)$$

$$D_0(y) - \frac{2}{3} E_0(y) = \frac{y(18+y-7y^2)}{12(y-1)^3} - \frac{y^2(12-10y+y^2)}{6(y-1)^4} \log y. \quad (46)$$

The dependence of the $\mu \rightarrow 3e$ decay rate factor $|C_{\mu 3e}|^2$ on the type I see-saw mass scale M_1 is shown in Fig. 5. At $M_1 = 100$ (1000) GeV we have: $|C_{\mu 3e}|^2 \cong 1.1$ (1639), i.e., $|C_{\mu 3e}|^2$ increases by 3 orders of magnitude when M_1 changes from 100 GeV to 1000 GeV. Using the quoted values of $|C_{\mu 3e}|^2$ we get the following constraint from the current limit on $\text{BR}(\mu \rightarrow 3e)$, eq. (4):

$$|(RV)_{\mu 1}^* (RV)_{e1}| \lesssim 2.1 \times 10^{-4} \text{ (} 5.3 \times 10^{-6} \text{) for } M_1 = 100 \text{ (1000) GeV.} \quad (47)$$

Thus, for $M_1 = 100$ GeV the constraint on $|(RV)_{\mu 1}^* (RV)_{e1}|$ obtained using the current experimental upper limit on $\text{BR}(\mu \rightarrow 3e)$ is by a factor of 2.5 less stringent than that obtained from the current upper limit on $\text{BR}(\mu \rightarrow e\gamma)$ (see eq. (29)), while for $M_1 = 1000$ GeV it is by a factor of 6 more stringent. However, for the two values of M_1 considered, the upper limit on $|(RV)_{\mu 1}^* (RV)_{e1}|$ from the current experimental bound on the $\mu - e$ conversion rate, eq. (5) is the most stringent. This is clearly seen in Fig. 2. It follows also from Fig. 2

that an experiment sensitive to a $\mu - e$ conversion rate $\text{CR}(\mu \text{Al} \rightarrow e \text{Al}) \approx 10^{-16}$, will probe smaller values of the product of couplings $|(RV)_{\mu 1}^*(RV)_{e 1}|$ than an experiment sensitive to $\text{BR}(\mu \rightarrow 3e) = 10^{-15}$.

In Fig. 4 we show the correlation between $\text{CR}(\mu \mathcal{N} \rightarrow e \mathcal{N})$ and $\text{BR}(\mu \rightarrow 3e)$ in the TeV scale see-saw model considered. As it follows from Fig. 4, the observation of the $\mu \rightarrow 3e$ decay or of the $\mu - e$ conversion in a given nucleus, combined with data on the ratio $\text{CR}(\mu \mathcal{N} \rightarrow e \mathcal{N})/\text{BR}(\mu \rightarrow 3e)$ would lead either to a unique determination of the type I see-saw scale M_1 , or to two values, or else to a relatively narrow interval of values, of M_1 compatible with the data. One can get the same type of information on the scale M_1 from data on the ratio $\text{BR}(\mu \rightarrow 3e)/\text{BR}(\mu \rightarrow e\gamma)$, provided at least one of the two decays $\mu \rightarrow e\gamma$ and $\mu \rightarrow 3e$ is observed.

It should be added finally that for $M_1 \gtrsim 100$ GeV we have: $\text{BR}(\mu \rightarrow 3e)/\text{BR}(\mu \rightarrow e\gamma) \gtrsim 0.067$. Thus, if it is experimentally established that $\text{BR}(\mu \rightarrow 3e)/\text{BR}(\mu \rightarrow e\gamma)$ is much smaller than the quoted lower bound, the model considered with $M_1 \gtrsim 100$ GeV will be ruled out. Such a result would be consistent also just with a see-saw scale $M_1 < 100$ GeV.

3 TeV Scale Type II See-Saw Model

We will consider in this section the type II see-saw [55] extension of the SM for the generation of the light neutrino masses. In its minimal formulation it includes one additional $SU(2)_L$ triplet Higgs field Δ , which has weak hypercharge $Y_W = 2$:

$$\Delta = \begin{pmatrix} \Delta^+/\sqrt{2} & \Delta^{++} \\ \Delta^0 & -\Delta^+/\sqrt{2} \end{pmatrix}. \quad (48)$$

The Lagrangian of the type II see-saw scenario, which is sometimes called also the ‘‘Higgs Triplet Model’’ (HTM), reads ⁷:

$$\mathcal{L}_{\text{seesaw}}^{\text{II}} = -M_\Delta^2 \text{Tr}(\Delta^\dagger \Delta) - \left(h_{\ell\ell'} \overline{\psi}_{\ell L}^C i\tau_2 \Delta \psi_{\ell' L} + \mu_\Delta H^T i\tau_2 \Delta^\dagger H + \text{h.c.} \right), \quad (49)$$

where $(\psi_{\ell L})^T \equiv (\nu_{\ell L}^T \ \ell_L^T)$, $\overline{\psi}_{\ell L}^C \equiv (-\nu_{\ell L}^T C^{-1} \ - \ \ell_L^T C^{-1})$, and H are, respectively, the SM lepton and Higgs doublets, C being the charge conjugation matrix, and μ_Δ is a real parameter characterising the soft explicit breaking of the total lepton charge conservation. We are interested in the low energy see-saw scenario, where the new physics scale M_Δ associated with the mass of Δ takes values $100 \text{ GeV} \lesssim M_\Delta \lesssim 1 \text{ TeV}$, which, in principle, can be probed by LHC [57].

The flavour structure of the Yukawa coupling matrix h and the size of the lepton charge soft breaking parameter μ_Δ are related to the light neutrino mass matrix m_ν , which is generated when the neutral component of Δ develops a ‘‘small’’ vev $v_\Delta \propto \mu_\Delta$. Indeed, setting $\Delta^0 = v_\Delta$ and $H^T = (0 \ v)^T$ with $v \simeq 174 \text{ GeV}$, from Lagrangian (49) one obtains:

$$(m_\nu)_{\ell\ell'} \equiv m_{\ell\ell'} \simeq 2 h_{\ell\ell'} v_\Delta. \quad (50)$$

⁷We do not give here, for simplicity, all the quadratic and quartic terms present in the scalar potential (see, e.g., [56]).

The matrix of Yukawa couplings $h_{\ell\ell'}$ is directly related to the PMNS neutrino mixing matrix $U_{\text{PMNS}} \equiv U$, which is unitary in this case:

$$h_{\ell\ell'} \equiv \frac{1}{2v_\Delta} (U^* \text{diag}(m_1, m_2, m_3) U^\dagger)_{\ell\ell'}. \quad (51)$$

An upper limit on v_Δ can be obtained from considering its effect on the parameter $\rho = M_W^2/M_Z^2 \cos^2 \theta_W$. In the SM, $\rho = 1$ at tree-level, while in the HTM one has

$$\rho \equiv 1 + \delta\rho = \frac{1 + 2x^2}{1 + 4x^2}, \quad x \equiv v_\Delta/v. \quad (52)$$

The measurement $\rho \approx 1$ leads to the bound $v_\Delta/v \lesssim 0.03$, or $v_\Delta < 5$ GeV (see, e.g., [58]).

As we will see, the amplitudes of the LFV processes $\mu \rightarrow e\gamma$, $\mu \rightarrow 3e$ and $\mu + \mathcal{N} \rightarrow e + \mathcal{N}$ in the model under discussion are proportional, to leading order, to a product of 2 elements of the Yukawa coupling matrix h . This implies that in order for the rates of the indicated LFV processes to be close to the existing upper limits and within the sensitivity of the ongoing MEG and the planned future experiments for $M_\Delta \sim (100 - 1000)$ GeV, the Higgs triplet vacuum expectation value v_Δ must be relatively small, roughly $v_\Delta \sim (1 - 100)$ eV. In the case of $M_\Delta \sim v = 174$ GeV we have $v_\Delta \cong \mu_\Delta$, while if $M_\Delta^2 \gg v^2$, then $v_\Delta \cong \mu_\Delta v^2/(2M_\Delta^2)$ (see, e.g., [56, 58]) with $v^2/(2M_\Delta^2) \cong 0.015$ for $M_\Delta = 1000$ GeV. Thus, in both cases a relatively small value of v_Δ implies that μ_Δ has also to be small. A nonzero but relatively small value of μ_Δ can be generated, e.g., at higher orders in perturbation theory [59] or in the context of theories with extra dimensions (see, e.g., [60]).

The physical singly-charged Higgs scalar field practically coincides with the triplet scalar field Δ^+ , the admixture of the doublet charged scalar field being suppressed by the factor v_Δ/v . The singly- and doubly- charged Higgs scalars Δ^+ and Δ^{++} have, in general, different masses [59, 61]: $m_{\Delta^+} \neq m_{\Delta^{++}}$. Both situations $m_{\Delta^+} > m_{\Delta^{++}}$ and $m_{\Delta^+} < m_{\Delta^{++}}$ are possible. In some cases, for simplicity, we will present numerical results for $m_{\Delta^+} \cong m_{\Delta^{++}} \equiv M_\Delta$, but one must keep in mind that m_{Δ^+} and $m_{\Delta^{++}}$ can have different values.

In the mass eigenstate basis, the effective charged lepton flavour changing operators arise at one-loop order from the exchange of the singly- and doubly-charged physical Higgs scalar fields. The corresponding effective low energy LFV Lagrangian, which contributes to the $\mu - e$ transition processes we are interested in, can be written in the form:

$$\begin{aligned} \mathcal{L}^{eff} = & -4 \frac{e G_F}{\sqrt{2}} (m_\mu A_R \bar{e} \sigma^{\alpha\beta} P_R \mu F_{\beta\alpha} + \text{h.c.}) \\ & - \frac{e^2 G_F}{\sqrt{2}} \left(A_L (-m_\mu^2) \bar{e} \gamma^\alpha P_L \mu \sum_{Q=u,d} q_Q \bar{Q} \gamma_\alpha Q + \text{h.c.} \right), \end{aligned} \quad (53)$$

where e is the proton charge, and $q_u = 2/3$ and $q_d = -1/3$ are the electric charges of the up and down quarks (in units of the proton charge). We obtain for the form factors $A_{R,L}$:

$$A_R = -\frac{1}{\sqrt{2} G_F} \frac{(h^\dagger h)_{e\mu}}{48\pi^2} \left(\frac{1}{8m_{\Delta^+}^2} + \frac{1}{m_{\Delta^{++}}^2} \right), \quad (54)$$

$$A_L(q^2) = -\frac{1}{\sqrt{2} G_F} \frac{h_{le}^* h_{l\mu}}{6\pi^2} \left(\frac{1}{12m_{\Delta^+}^2} + \frac{1}{m_{\Delta^{++}}^2} f\left(\frac{-q^2}{m_{\Delta^{++}}^2}, \frac{m_l^2}{m_{\Delta^{++}}^2}\right) \right), \quad (55)$$

m_l being the mass of the charged lepton l , $l = e, \mu, \tau$. In the limit where the transition is dominated by the exchange of a virtual doubly charged scalar Δ^{++} , these expressions reduce to those obtained in [62, 63]. The term with the form factor A_R in eq. (53) generates the $\mu \rightarrow e\gamma$ decay amplitude. It corresponds to the contribution of the one loop diagrams with virtual neutrino and Δ^+ [64] and with virtual charged lepton and Δ^{++} [62] (see also [65]). The second term involving the form factor A_L , together with A_R , generates the $\mu - e$ conversion amplitude. The loop function $f(r, s_l)$ is well known [63]:

$$f(r, s_l) = \frac{4s_l}{r} + \log(s_l) + \left(1 - \frac{2s_l}{r}\right) \sqrt{1 + \frac{4s_l}{r}} \log \frac{\sqrt{r} + \sqrt{r + 4s_l}}{\sqrt{r} - \sqrt{r + 4s_l}}. \quad (56)$$

Notice that in the limit in which the charged lepton masses m_l are much smaller than the doubly-charged scalar mass $m_{\Delta^{++}}$, one has $f(r, s_l) \simeq \log(r) = \log(m_\mu^2/m_{\Delta^{++}}^2)$. For $m_{\Delta^{++}} = (100 - 1000)$ GeV, this is an excellent approximation for $f(r, s_e)$, but cannot be used for $f(r, s_\mu)$ and $f(r, s_\tau)$. The ratios $f(r, s_e)/f(r, s_\mu)$ and $f(r, s_e)/f(r, s_\tau)$ change relatively little when $m_{\Delta^{++}}$ increases from 100 GeV to 1000 GeV, and at $m_{\Delta^{++}} = 100$ (1000) GeV take the values: $f(r, s_e)/f(r, s_\mu) \cong 1.2$ (1.1) and $f(r, s_e)/f(r, s_\tau) \cong 2.1$ (1.7). More generally, $f(r, s_l)$, $l = e, \mu, \tau$, are monotonically (slowly) decreasing functions of $m_{\Delta^{++}}$ ⁸: for $m_{\Delta^{++}} = 100$ (1000) GeV we have, e.g., $f(r, s_e) \cong -13.7$ (-18.3).

3.1 The $\mu \rightarrow e\gamma$ Decay

Using eqs. (53) and (54) we get for the $\mu \rightarrow e\gamma$ decay branching ratio in the case under discussion [64, 56]:

$$\text{BR}(\mu \rightarrow e\gamma) \cong 384 \pi^2 (4\pi \alpha_{\text{em}}) |A_R|^2 = \frac{\alpha_{\text{em}}}{192 \pi} \frac{|(h^\dagger h)_{e\mu}|^2}{G_F^2} \left(\frac{1}{m_{\Delta^+}^2} + \frac{8}{m_{\Delta^{++}}^2} \right)^2. \quad (57)$$

For $m_{\Delta^+} \cong m_{\Delta^{++}} \equiv M_\Delta$, the upper limit on $\text{BR}(\mu \rightarrow e\gamma)$ reported by the MEG experiment, eq. (3), implies the following upper bound on $|(h^\dagger h)_{e\mu}|$:

$$|(h^\dagger h)_{e\mu}| < 5.8 \times 10^{-6} \left(\frac{M_\Delta}{100 \text{ GeV}} \right)^2. \quad (58)$$

One can use this upper bound, in particular, to obtain a lower bound on the vacuum expectation value of Δ^0 , v_Δ . Indeed, from eq. (51) it is not difficult to get:

$$|(h^\dagger h)_{e\mu}| = \frac{1}{4v_\Delta^2} \left| U_{e2} U_{2\mu}^\dagger \Delta m_{21}^2 + U_{e3} U_{3\mu}^\dagger \Delta m_{31}^2 \right|, \quad (59)$$

where we have used the unitarity of U . The above expression for $|(h^\dagger h)_{e\mu}|$ is exact. It follows from eq. (59) that the prediction for $|(h^\dagger h)_{e\mu}|$, and thus for $\text{BR}(\mu \rightarrow e\gamma)$, depends, in general, on the Dirac CPV phase δ of the standard parametrisation of the PMNS matrix U (see eq. (21)). For the best fit values of $\sin^2 \theta_{13} = 0.0236$ and of the other neutrino oscillation parameters listed in Table 1, the term $\propto \Delta m_{21}^2$ in eq. (59) is approximately a factor of 10 smaller than the term $\propto \Delta m_{31}^2$. In this case $\text{BR}(\mu \rightarrow e\gamma)$ exhibits a relatively

⁸Note that we have $f(r, s_l) < 0$, $l = e, \mu, \tau$.

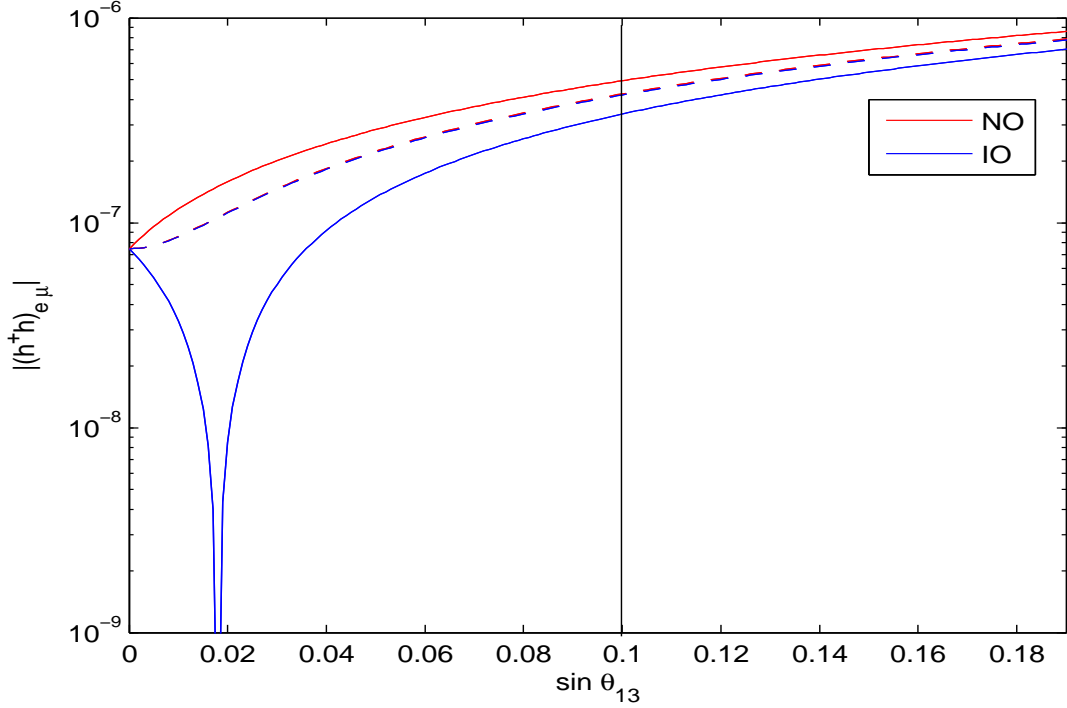


Figure 6: The dependence of $|(h^\dagger h)_{e\mu}|$ on $\sin \theta_{13}$ for $v_\Delta = 9.5$ eV and $\delta = 0$ (solid lines) and $\delta = \pi/2$ (dashed line). The other neutrino oscillation parameters are set to their best fit values given in Table 1. The vertical line corresponds to the current 3σ allowed minimal value of $\sin \theta_{13}$ (see eq. (1)).

weak dependence on the type of the neutrino mass spectrum and on the Dirac phase δ . Neglecting the term $\propto \Delta m_{21}^2$, we obtain from (58) and (59):

$$v_\Delta > 2.1 \times 10^2 |s_{13} s_{23} \Delta m_{31}^2|^{\frac{1}{2}} \left(\frac{100 \text{ GeV}}{M_\Delta} \right) \cong 3.0 \text{ eV} \left(\frac{100 \text{ GeV}}{M_\Delta} \right). \quad (60)$$

For the 3σ allowed ranges of values of $\sin^2 2\theta_{13}$ given in eq. (1) and of the other neutrino oscillation parameters quoted in Table 1, the absolute lower bound on v_Δ corresponds approximately to $v_\Delta > 1.5 \text{ eV} (100 \text{ GeV})/M_\Delta$ and is reached in the case of $\Delta m_{31}^2 > 0$ ($\Delta m_{31}^2 < 0$) for $\delta = \pi$ (0).

We note further that if $\delta \cong \pi/2$ ($3\pi/2$), the term $\propto \Delta m_{21}^2$ in the expression for $|(h^\dagger h)_{e\mu}|$ (and thus for $\text{BR}(\mu \rightarrow e\gamma)$) always plays a subdominant role as long as the other neutrino oscillation parameters lie in their currently allowed 3σ ranges. Therefore in this case the dependence of $\text{BR}(\mu \rightarrow e\gamma)$ on the type of neutrino mass spectrum is negligible. The specific features of the predictions for $|(h^\dagger h)_{e\mu}|$ discussed above are illustrated in Fig. 6.

Exploiting the fact that $v_\Delta^2 |(h^\dagger h)_{e\mu}|$ is known with a rather good precision, we can write:

$$\text{BR}(\mu \rightarrow e\gamma) \cong 2.7 \times 10^{-10} \left(\frac{1 \text{ eV}}{v_\Delta} \right)^4 \left(\frac{100 \text{ GeV}}{M_\Delta} \right)^4, \quad (61)$$

where we have used eq. (57) and the best fit values of the neutrino oscillation parameters.

It follows from eq. (61) that for the values of v_Δ and M_Δ (or $m_{\Delta+}$ and/or $m_{\Delta++}$) of interest, $\text{BR}(\mu \rightarrow e\gamma)$ can have a value within the projected sensitivity of the ongoing MEG experiment.

3.2 The $\mu \rightarrow 3e$ decay

In the TeV scale type II see-saw scenario, the $\mu \rightarrow 3e$ decay amplitude is generated at the tree level by the diagram with exchange of a virtual doubly-charged Higgs boson Δ^{++} . The branching ratio can be easily calculated (see, e.g., [62, 65]):

$$\text{BR}(\mu \rightarrow 3e) = \frac{1}{G_F^2} \frac{|(h^\dagger)_{ee}(h)_{\mu e}|^2}{m_{\Delta^{++}}^4} = \frac{1}{G_F^2 m_{\Delta^{++}}^4} \frac{|m_{ee}^* m_{\mu e}|^2}{16 v_\Delta^4}, \quad (62)$$

where we have used eq. (50). From the present limit $\text{BR}(\mu \rightarrow 3e) < 10^{-12}$, one can obtain the following constraint on $|(h^\dagger)_{ee}(h)_{\mu e}|$:

$$|(h^\dagger)_{ee}(h)_{\mu e}| < 1.2 \times 10^{-7} \left(\frac{m_{\Delta^{++}}}{100 \text{ GeV}} \right)^2. \quad (63)$$

In the model under discussion, $\text{BR}(\mu \rightarrow 3e)$ depends on the factor $|m_{ee}^* m_{\mu e}|$, which involves the product of two elements of the neutrino Majorana mass matrix, on the neutrino mass spectrum and on the Majorana and Dirac CPV phases in the PMNS matrix U . For the values of $m_{\Delta+}$ and $m_{\Delta++}$ in the range of $\sim (100 - 1000)$ GeV and of $v_\Delta \ll 1$ MeV of interest, m_{ee} practically coincides with the effective Majorana mass in neutrinoless double beta $((\beta\beta)_{0\nu-})$ decay (see, e.g., [65, 66, 67]), $\langle m \rangle$:

$$|m_{ee}| = \left| \sum_{j=1}^3 m_j U_{ej}^2 \right| \cong |\langle m \rangle|. \quad (64)$$

Depending on the type of neutrino mass spectrum, the value of the lightest neutrino mass and on the values of the CPV Majorana and Dirac phases in the PMNS matrix, $|m_{ee}|$ can take any value between 0 and m_0 , where $m_0 = m_1 \cong m_2 \cong m_3$ is the value of the neutrino masses in the case of quasi-degenerate (QD) spectrum, $m_0 \gtrsim 0.1$ eV (see, e.g., [66]). It follows from the searches for the $(\beta\beta)_{0\nu}$ -decay that $|m_{ee}| \lesssim m_0 \lesssim 1$ eV, while the cosmological constraints on the sum of the neutrino masses imply $m_0 \lesssim 0.3$ eV (see, e.g., [1]). As is well known, the $(\beta\beta)_{0\nu}$ -decay is claimed to have been observed in [68, 69], with the reported half-life corresponding to [69] $|m_{ee}| = 0.32 \pm 0.03$ eV. This claim will be tested in a new generation of $(\beta\beta)_{0\nu}$ -decay experiments which either are already taking data or are in preparation at present (see, e.g., [1, 70]).

In the case of NH light neutrino mass spectrum with $m_1 \ll 10^{-4}$ eV, $|m_{ee}|$ lies in the interval 3.6×10^{-4} eV $\lesssim |m_{ee}| \lesssim 5.2 \times 10^{-3}$ eV. This interval was obtained by taking into account the 3σ allowed ranges of values of $\sin^2 \theta_{13}$ (eq. (1)), $\sin^2 \theta_{12}$, $\sin^2 \theta_{23}$ and Δm_{\odot}^2 and Δm_{A}^2 . For the best fit values (b.f.v.) of the latter we get ⁹: 1.45×10^{-3} eV $\lesssim |m_{ee}| \lesssim 3.75 \times 10^{-3}$ eV. The minimal and the maximal values correspond to the combination of the CPV

⁹The numerical values quoted further in this subsection are obtained for the indicated best fit values of the neutrino oscillation parameters, unless otherwise stated.

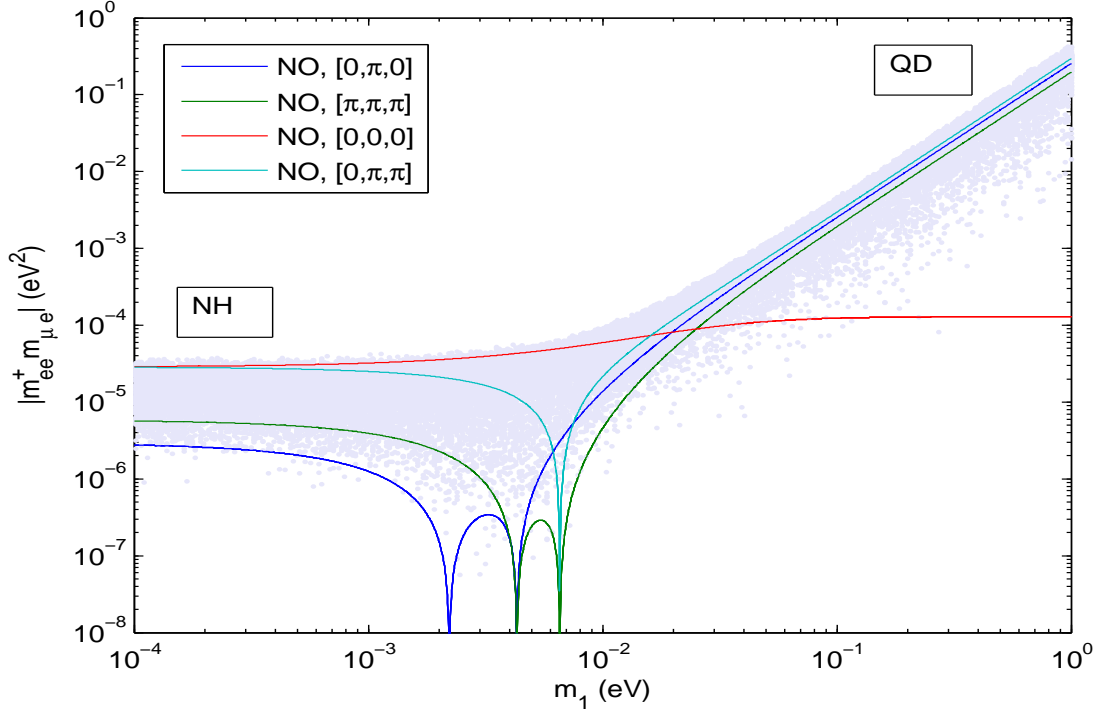


Figure 7: The dependence of $|m_{ee}^* m_{\mu e}|$ on the lightest neutrino mass m_1 in the case of neutrino mass spectrum with normal ordering ($\Delta m_A^2 > 0$), for four sets of values of the Dirac and the two Majorana CPV phases, $[\delta, \alpha_{21}, \alpha_{31}]$. The depicted curves correspond to the best fit values of $\sin \theta_{13}$ (eq. (1)) and of the other neutrino oscillation parameters given in Table 1. The scattered points are obtained by varying the neutrino oscillation parameters within their corresponding 3σ intervals and giving random values to the CPV Dirac and Majorana phases.

phases $(\alpha_{21} - \alpha_{31} + 2\delta) = \pi$ and 0 , respectively. However, for $m_1 \gtrsim 10^{-4}$ eV, one can have $|m_{ee}| = 0$ for specific values of m_1 if the CPV phases α_{21} and $\alpha_{31} - 2\delta$ possess the CP conserving values $\alpha_{21} = \pi$ and $(\alpha_{31} - 2\delta) = 0, \pi$ (see, e.g., [17]): for the $[\pi, 0]$ combination this occurs at $m_1 \cong 2.3 \times 10^{-3}$ eV, while in the case of the $[\pi, \pi]$ one we have $|m_{ee}| = 0$ at $m_1 \cong 6.5 \times 10^{-3}$ eV. If the light neutrino mass spectrum is with inverted ordering ($\Delta m_A^2 \equiv \Delta m_{32}^2 < 0$, $m_3 < m_1 < m_2$) or of inverted hierarchical (IH) type ($m_3 \ll m_1 < m_2$), we have [71] $|m_{ee}| \gtrsim \sqrt{|\Delta m_A^2| + m_3^2} \cos 2\theta_{12} \gtrsim 1.27 \times 10^{-2}$ eV, while in the case of QD spectrum, $|m_{ee}| \gtrsim m_0 \cos 2\theta_{12} \gtrsim 2.8 \times 10^{-2}$ eV, where we used the 3σ minimal allowed values of $|\Delta m_A^2|$ and $\cos 2\theta_{12}$.

We consider next briefly the dependence of the neutrino mass matrix element $|m_{\mu e}|$ on the type of the neutrino mass spectrum and on the CPV Majorana and Dirac phases. In the case of NH spectrum with $m_1 = 0$, the maximal value of $|m_{\mu e}|$ is obtained for $\alpha_{31} - \alpha_{21} = \delta$, $\delta = \pi$, and reads: $\max(|m_{\mu e}|) \cong 8.1 \times 10^{-3}$ eV. We get $|m_{\mu e}| = 0$ for $\alpha_{21} = \pi$, $\delta = 0$ (π) and $\alpha_{31} = 0$ (π). As can be shown, for each of these two sets of values of the CPV phases, the zero takes place at essentially the same value of $m_1 \cong 4.3 \times 10^{-3}$ eV (Fig. 7). If the neutrino mass spectrum is of the IH type with negligible $m_3 \cong 0$, the maximal value of $|m_{\mu e}|$ corresponds

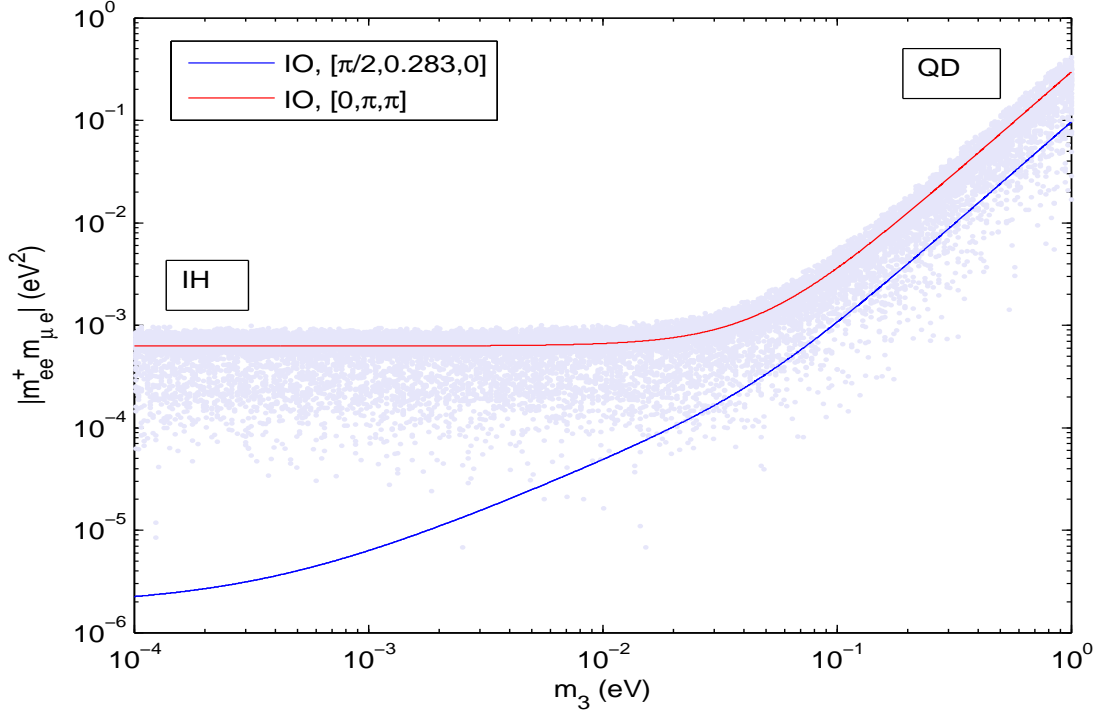


Figure 8: The same as in Fig. 7 in the case of a light neutrino mass spectrum with inverted ordering ($\Delta m_A^2 < 0$) (see text for details).

to $\delta = 0$ and $\alpha_{21} = \pi$ and is given by $\max(|m_{\mu e}|) \cong \sqrt{|\Delta m_A^2|} c_{13}(c_{23} \sin 2\theta_{12} + s_{23}s_{13} \cos 2\theta_{12})$. The element $|m_{\mu e}|$ is strongly suppressed, i.e., we have $|m_{\mu e}| \ll \max(|m_{\mu e}|)$, for $\delta \cong \pi/2$ and a value of the Majorana phase α_{21} which is determined by the equation:

$$c_{23} c_{12} s_{12} \sin \alpha_{21} \cong (c_{12}^2 + s_{12}^2 \cos \alpha_{21}) s_{23} s_{13}. \quad (65)$$

For the b.f.v. of the neutrino mixing angles this equation is satisfied for $\alpha_{21} \cong 0.283$.

The properties of $|m_{ee}|$ and $|m_{\mu e}|$ described above allow us to understand most of the specific features of the dependence of the quantity $|m_{ee}^* m_{\mu e}|$ of interest on the the neutrino mass spectrum and the leptonic CPV phases. For NH spectrum and negligible $m_1 \cong 0$, the maximum of the latter is obtained for $\alpha_{31} - \alpha_{21} = \delta = 0$ and is given by:

$$\max(|m_{ee}^* m_{\mu e}|) = \left| (m_2 s_{12}^2 c_{13}^2 + m_3 s_{13}^2) c_{13} (m_2 s_{12} (c_{12} c_{23} - s_{12} s_{23} s_{13}) + m_3 s_{23} s_{13}) \right|, \quad (66)$$

with $m_2 = \sqrt{\Delta m_{\odot}^2}$ and $m_3 = \sqrt{\Delta m_A^2}$. Using the b.f.v. of the neutrino oscillation parameters we get $\max(|m_{ee}^* m_{\mu e}|) \cong 2.9 \times 10^{-5} \text{ eV}^2$ (see Fig. 7). This implies $\text{BR}(\mu \rightarrow 3e) \lesssim 6 \times 10^{-9} (1 \text{ eV}/v_{\Delta})^4 (100 \text{ GeV}/m_{\Delta^{++}})^4$. In the case of NH spectrum and non-negligible m_1 we have $|m_{ee}^* m_{\mu e}| = 0$ for the values of the CPV phases and m_1 discussed above, for which either $|m_{ee}| = 0$ or $|m_{\mu e}| = 0$. The scattered points in Fig. 7 correspond to the possible values the quantity $|m_{ee}^* m_{\mu e}|$ can assume when varying the neutrino oscillation parameters within their corresponding 3σ intervals and giving random values to the CPV Dirac and Majorana phases from the interval $[0, 2\pi]$.

The maximum of $|m_{ee}m_{\mu e}|$ for the IH spectrum with a negligible m_3 is reached for $\delta = 0$ and $\alpha_{21} = \pi$, and reads:

$$\max(|m_{ee}^*m_{\mu e}|) \cong |\Delta m_A^2| c_{13}^3 \left(\frac{1}{2} c_{23} \sin 4\theta_{12} + s_{23} s_{13} \cos^2 2\theta_{12} \right). \quad (67)$$

Numerically this gives $\max(|m_{ee}m_{\mu e}|) \cong 6.1 \times 10^{-4} \text{ eV}^2$ (Fig. 8). For $\text{BR}(\mu \rightarrow 3e)$ we thus obtain: $\text{BR}(\mu \rightarrow 3e) \lesssim 2.4 \times 10^{-6} (1 \text{ eV}/v_\Delta)^4 (100 \text{ GeV}/m_{\Delta^{++}})^4$. One can have $|m_{ee}m_{\mu e}| \ll \max(|m_{ee}m_{\mu e}|)$ in the case of IH spectrum with $m_3 = 0$ for, e.g., $\delta \cong \pi/2$ and $\alpha_{21} \cong 0.283$, for which $|m_{\mu e}|$ has a minimum. For the indicated values of the phases we find: $|m_{ee}m_{\mu e}| \cong 1.2 \times 10^{-6} \text{ eV}^2$ (see Fig. 8). Similarly to the case of a neutrino mass spectrum with normal ordering discussed above, we show in Fig. 8 the range of values the LFV term $|m_{ee}m_{\mu e}|$ can assume (scattered points).

Finally, in the case of QD spectrum, $|m_{ee}m_{\mu e}|$ will be relatively strongly suppressed with respect to its possible maximal value for this spectrum (i.e., we will have $|m_{ee}m_{\mu e}| \ll \max(|m_{ee}^*m_{\mu e}|)$) if, e.g., the Majorana and Dirac phases are zero, thus conserving the CP symmetry: $\alpha_{21} = \alpha_{31} = \delta = 0$. Then one has: $|m_{ee}m_{\mu e}| \cong |\Delta m_A^2| s_{13} s_{23} c_{13}/2 \cong 1.2 \times 10^{-4} \text{ eV}^2$. Note that this value is still larger than the maximal value of $|m_{ee}m_{\mu e}|$ for the NH neutrino mass spectrum with a negligible m_1 (see Fig. 7). The maximum of $|m_{ee}m_{\mu e}|$ takes place for another set of CP conserving values of the Majorana and Dirac phases: $\alpha_{21} = \alpha_{31} = \pi$ and $\delta = 0$. At the maximum we have:

$$\max(|m_{ee}^*m_{\mu e}|) \cong m_0^2 (c_{13}^3 \cos 2\theta_{12} - s_{13}^2) c_{13} (c_{23} \sin 2\theta_{12} + 2 c_{12}^2 s_{23} s_{13}), \quad m_0 \gtrsim 0.1 \text{ eV}. \quad (68)$$

For the b.f.v. of the neutrino mixing angles we get $\max(|m_{ee}^*m_{\mu e}|) \cong 0.3 m_0^2$. For $m_0 \lesssim 0.3 \text{ eV}$ this implies $\max(|m_{ee}^*m_{\mu e}|) \lesssim 2.7 \times 10^{-2} \text{ eV}^2$, leading to an upper bound on $\text{BR}(\mu \rightarrow 3e)$, which is by a factor approximately of 4.1×10^3 larger than in the case of IH spectrum.

The features of $|m_{ee}m_{\mu e}|$ discussed above are illustrated in Figs. 7 and 8.

It should be clear from the preceding discussion that in the case of the type II see-saw model considered, the value of the quantity $|(h^\dagger)_{ee}(h)_{\mu e}|^2 \propto |m_{ee}^*m_{\mu e}|^2$, and thus the prediction for $\text{BR}(\mu \rightarrow 3e)$, depends very strongly on the type of neutrino mass spectrum. For a given spectrum, it exhibits also a very strong dependence on the values of the Majorana and Dirac CPV phases α_{21} , α_{31} and δ , as well as on the value of the lightest neutrino mass, $\min(m_j)$. As a consequence, the prediction for $\text{BR}(\mu \rightarrow 3e)$ for given v_Δ and $m_{\Delta^{++}}$ can vary by a few to several orders of magnitude when one varies the values of $\min(m_j)$ and of the CPV phases. Nevertheless, for all possible types of neutrino mass spectrum - NH, IH, QD, etc., there are relatively large regions of the parameter space of the model where $\text{BR}(\mu \rightarrow 3e)$ has a value within the sensitivity of the planned experimental searches for the $\mu \rightarrow 3e$ decay [33]. The region of interest for the NH spectrum is considerably smaller than those for the IH and QD spectra. In the case NO spectrum ($\Delta m_A^2 > 0$), $\text{BR}(\mu \rightarrow 3e)$ can be strongly suppressed for certain values of the lightest neutrino mass m_1 from the interval $\sim (2 \times 10^{-3} - 10^{-2}) \text{ eV}$ (Fig. 7). For the IO spectrum ($\Delta m_A^2 < 0$), a similar suppression can take place for $m_3 \ll 10^{-2} \text{ eV}$ (Fig. 8). In the cases when $|m_{ee}^*m_{\mu e}|^2$ is very strongly suppressed, the one-loop corrections to the $\mu \rightarrow 3e$ decay amplitude should be taken into account since they might give a larger contribution than that of the tree level diagram we are considering. The analysis of this case, however, is beyond the scope of the present investigation.

\mathcal{N}	$D m_\mu^{-5/2}$	$V^{(p)} m_\mu^{-5/2}$	$V^{(n)} m_\mu^{-5/2}$	$\Gamma_{\text{capt}} (10^6 \text{ s}^{-1})$
$^{48}_{22}\text{Ti}$	0.0864	0.0396	0.0468	2.590
$^{27}_{13}\text{Al}$	0.0362	0.0161	0.0173	0.7054
$^{197}_{79}\text{Au}$	0.189	0.0974	0.146	13.07

Table 2: Nuclear parameters related to $\mu - e$ conversion in $^{48}_{22}\text{Ti}$, $^{27}_{13}\text{Al}$ and $^{197}_{79}\text{Au}$. The numerical values of the overlap integrals D , $V^{(p)}$ and $V^{(n)}$ are taken from [72].

3.3 The $\mu - e$ Conversion in Nuclei

Consider next the $\mu - e$ conversion in a generic nucleus \mathcal{N} . We parametrise the corresponding conversion rate following the effective field theory approach developed in [72]. Taking into account the interaction Lagrangian (53), we get in the type II see-saw scenario

$$\text{CR}(\mu \mathcal{N} \rightarrow e \mathcal{N}) \cong (4\pi\alpha_{\text{em}})^2 \frac{2 G_F^2}{\Gamma_{\text{capt}}} \left| A_R \frac{D}{\sqrt{4\pi\alpha_{\text{em}}}} + (2q_u + q_d) A_L V^{(p)} \right|^2. \quad (69)$$

The parameters D and $V^{(p)}$ represent overlap integrals of the muon and electron wave functions and are related to the effective dipole and vector type operators in the interaction Lagrangian, respectively (see, *e.g.* [72]).

In the case of a light nucleus, *i.e.* for $Z \lesssim 30$, one has with a good approximation $D \simeq 8 \sqrt{4\pi\alpha_{\text{em}}} V^{(p)}$, with the vector type overlap integral of the proton, $V^{(p)}$, given by [72]:

$$V^{(p)} \simeq \frac{1}{4\pi} m_\mu^{5/2} \alpha_{\text{em}}^{3/2} Z_{\text{eff}}^2 Z^{1/2} F(-m_\mu^2), \quad (70)$$

where $F(q^2)$ is the form factor of the nucleus. The parameters $D m_\mu^{-5/2}$, $V^{(p)} m_\mu^{-5/2}$ and Γ_{capt} for $^{48}_{22}\text{Ti}$, $^{27}_{13}\text{Al}$ and $^{197}_{79}\text{Au}$ are given in Table 2. Using the result for D quoted above, eqs. (54), (55) and (70), the conversion rate (69) can be written as

$$\begin{aligned} \text{CR}(\mu \mathcal{N} \rightarrow e \mathcal{N}) \cong & \frac{\alpha_{\text{em}}^5}{36 \pi^4} \frac{m_\mu^5}{\Gamma_{\text{capt}}} Z_{\text{eff}}^4 Z F^2(-m_\mu^2) \left| (h^\dagger h)_{e\mu} \left[\frac{5}{24 m_{\Delta+}^2} + \frac{1}{m_{\Delta++}^2} \right] \right. \\ & \left. + \frac{1}{m_{\Delta++}^2} \sum_{l=e,\mu,\tau} h_{el}^\dagger f(r, s_l) h_{l\mu} \right|^2. \end{aligned} \quad (71)$$

Thus, assuming $m_{\Delta+} \cong m_{\Delta++} \equiv M_\Delta$, we have $\text{CR}(\mu \mathcal{N} \rightarrow e \mathcal{N}) \propto |C_{\mu e}^{(II)}|^2$, where

$$C_{\mu e}^{(II)} \equiv \frac{1}{4v_\Delta^2} \left[\frac{29}{24} (m^\dagger m)_{e\mu} + \sum_{l=e,\mu,\tau} m_{el}^\dagger f(r, s_l) m_{l\mu} \right], \quad (72)$$

and we have used eq. (50). The upper limit on the $\mu - e$ conversion rate in Ti, eq. (5), leads to the following upper limit on $|C_{\mu e}^{(II)}|$:

$$|C_{\mu e}^{(II)}| < 1.24 \times 10^{-4} \left(\frac{M_\Delta}{100 \text{ GeV}} \right)^2. \quad (73)$$

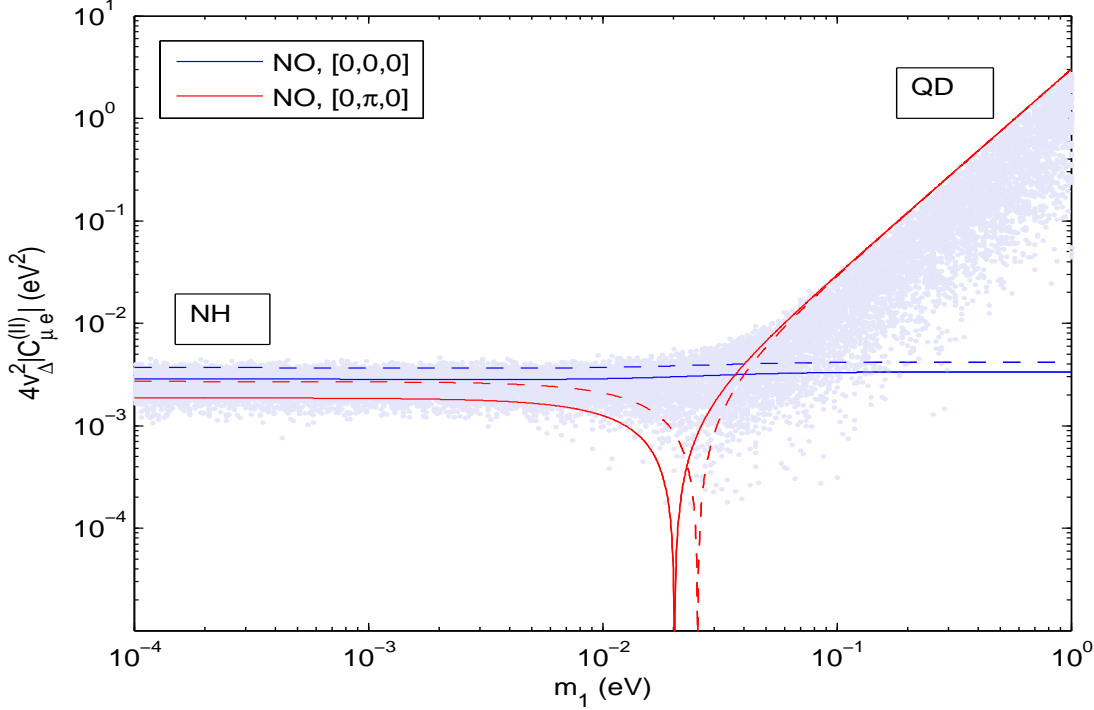


Figure 9: The dependence of $4v_\Delta^2 |C_{\mu e}^{(II)}|$ (given in eV^2) on the lightest neutrino mass m_1 in the case of neutrino mass spectrum with normal ordering ($\Delta m_A^2 > 0$), for two sets of values of the Dirac and the two Majorana CPV phases, $[\delta, \alpha_{21}, \alpha_{31}]$ and $M_\Delta = 200$ (1000) GeV, plain (dashed) curves. The figure is obtained for the best fit values of $\sin \theta_{13}$ (eq. (1)) and of the other neutrino oscillation parameters given in Table 1 (see text for details).

In obtaining it we have used the values of Γ_{capt} , Z_{eff} , Z and $F(-m_\mu^2)$ for Ti given in subsection 2.2. An experiment sensitive to $\text{CR}(\mu \text{ Ti} \rightarrow e \text{ Ti}) \approx 10^{-18}$ [31] will be able to probe values of $|C_{\mu e}^{(II)}| \gtrsim 5.8 \times 10^{-8} (M_\Delta / (100 \text{ GeV}))^2$.

The $\mu - e$ conversion rate in a given nucleus depends through the quantity $C_{\mu e}^{(II)}$, on the type of neutrino mass spectrum and the Majorana and Dirac CPV phases in the PMNS matrix. Using the b.f.v. of the neutrino oscillation parameters and performing a scan over the values of the CPV phases and the lightest neutrino mass, which in the cases of NO ($\Delta m_A^2 > 0$) and IO ($\Delta m_A^2 < 0$) spectra was varied in the intervals $(10^{-4} - 1)$ eV and $(10^{-5} - 1)$ eV, respectively, we have identified the possible ranges of values of $4v_\Delta^2 |C_{\mu e}^{(II)}|$. The latter are shown in Figs. (9) and (10).

For $M_\Delta = 200$ (1000) GeV and NH spectrum with negligible m_1 ($m_1 \ll 10^{-3}$ eV), the maximal value of $4v_\Delta^2 |C_{\mu e}^{(II)}|$ occurs for $[\delta, \alpha_{21}, \alpha_{31}] = [0, 0, 0]$ and at the maximum we have $4v_\Delta^2 |C_{\mu e}^{(II)}| \cong 2.9$ (3.8) $\times 10^{-3}$ eV^2 . For values of the CPV phases $[\delta, \alpha_{21}, \alpha_{31}] = [0, \pi, 0]$ and $M_\Delta = 200$ GeV, $4v_\Delta^2 |C_{\mu e}^{(II)}|$ goes through zero at $m_1 \cong 2 \times 10^{-2}$ eV (Fig. 9). In the case of a larger charged scalar mass, *i.e.* $M_\Delta = 1000$ GeV, such cancellation occurs at a different value of the lightest neutrino mass, mainly $m_1 = 0.025$ eV.

The maximum of $4v_\Delta^2 |C_{\mu e}^{(II)}|$ in the case of IH spectrum with negligible m_3 , occurs for

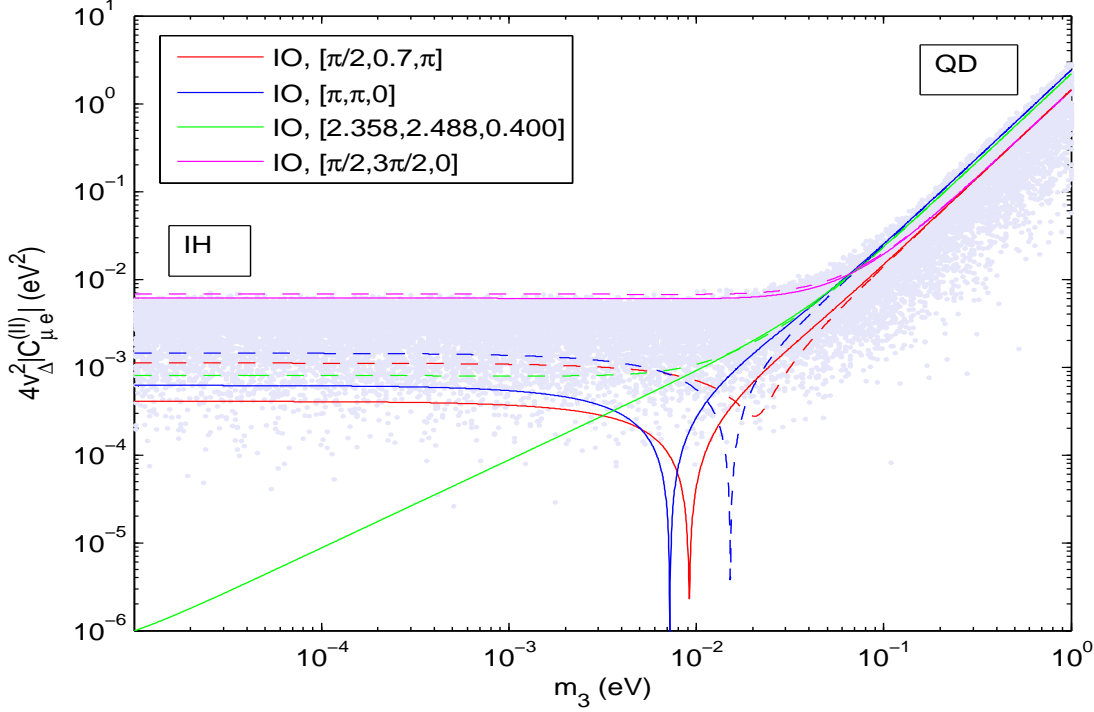


Figure 10: The same as in Fig. 9 in the case of a light neutrino mass spectrum with inverted ordering.

maximal CPV phases: $[\delta, \alpha_{21}, \alpha_{31}] = [\pi/2, 3\pi/2, 0]$. At the maximum in this case one has $4v_\Delta^2 |C_{\mu e}^{(II)}| \cong 6 \text{ (7)} \times 10^{-3} \text{ eV}^2$ for $M_\Delta = 200 \text{ (1000)} \text{ GeV}$. As Fig. 10 shows, for other sets of values of the CPV phases, $4v_\Delta^2 |C_{\mu e}^{(II)}|$ can be much smaller. Taking again CP conserving phases, *e.g.* $[\pi, \pi, 0]$, one can get a strong suppression of the branching ratio for $m_3 = 7.2 \text{ (15)} \times 10^{-3} \text{ eV}$ and $M_\Delta = 200 \text{ (1000)} \text{ GeV}$. Allowing $\sin \theta_{13}$ to take values other than the best fit one, we find that $4v_\Delta^2 |C_{\mu e}^{(II)}|$ can even go through zero at, *e.g.*, $[\delta, \alpha_{21}, \alpha_{31}] = [\pi, \pi, \pi/2]$ for $\sin \theta_{13} \cong 0.137$, which lies within the 2σ allowed region. In Fig. 10 we report other examples in which the CPV phases in the PMNS matrix take different sets of CP violating values and the quantity $4v_\Delta^2 |C_{\mu e}^{(II)}|$ (and the conversion rate) can vary by several orders of magnitude for specific values of the lightest neutrino mass m_3 and the see-saw mass scale M_Δ .

If the neutrino mass spectrum is quasi-degenerate, $m_{1,2,3} \cong m_0 \gtrsim 0.1 \text{ eV}$, we have for $m_0 \lesssim 0.3 \text{ eV}$: $2.8 \times 10^{-3} \text{ eV}^2 \lesssim 4v_\Delta^2 |C_{\mu e}^{(II)}| \lesssim 0.4 \text{ eV}^2$. The minimal value corresponds to $\Delta m_A^2 > 0$ (NO spectrum) and $[\delta, \alpha_{21}, \alpha_{31}] = [\pi, 0, 0]$; for *e.g.* $[\delta, \alpha_{21}, \alpha_{31}] = [0, 0, 0]$ and $M_\Delta = 200 \text{ GeV}$ we get in the QD region $4v_\Delta^2 |C_{\mu e}^{(II)}| \cong 3.3 \times 10^{-3} \text{ eV}^2$ (Fig. 9).

Finally, the scattered points in Figs. 9 and 10 are obtained by varying all the neutrino oscillation parameters within the corresponding 3σ intervals and allowing for arbitrary values of the Dirac and Majorana phases in the interval $[0, 2\pi]$.

We remark that the previous estimates, as well as Figs 9 and 10, were realized under the assumption that the singly- and doubly-charged scalars have masses of the same order,

i.e. $m_{\Delta^+} \cong m_{\Delta^{++}} \equiv M_{\Delta}$. The case in which the dominant contribution to the conversion amplitude is provided by the exchange of Δ^{++} , *i.e.* for $m_{\Delta^+} \gg m_{\Delta^{++}} \gtrsim 100$ GeV, shows similar features: the upper limits of the conversion ratio in the cases of NO and IO spectra are unchanged and a strong suppression can occur for specific values of the CPV phases and $\min(m_j)$. Taking, instead, the opposite limit $m_{\Delta^{++}} \gg m_{\Delta^+}$, with $m_{\Delta^+} = (100 - 1000)$ GeV, the dominant contribution to the $\mu - e$ conversion amplitude is given by the exchange of the singly-charged scalar, therefore we have: $|C_{\mu e}^{(II)}| \propto |(h^\dagger h)_{e\mu}|$. As it was pointed out in subsection 3.1, $|(h^\dagger h)_{e\mu}|$ shows a relative weak dependance on the type of neutrino mass spectrum and on the CPV phases in the PMNS matrix. Moreover, no suppression of the conversion amplitude occurs if $\sin(\theta_{13})$ is taken within the current 3σ experimental bound (see Fig. 6). In this case, from the best experimental upper bound on the conversion rate in Ti, $\text{CR}(\mu \text{ Ti} \rightarrow e \text{ Ti}) < 4.3 \times 10^{-12}$, we get the constraint:

$$|(h^\dagger h)_{e\mu}| < 6 \times 10^{-4} \left(\frac{m_{\Delta^+}}{100 \text{ GeV}} \right)^2, \quad (74)$$

which provides a weaker bound with respect to that obtained from the $\mu \rightarrow e\gamma$ decay (see eq. (58)). A $\mu - e$ conversion experiment sensitive to *i.e.* $\text{CR}(\mu \text{ Ti} \rightarrow e \text{ Ti}) \approx 10^{-18}$, can probe values of $|(h^\dagger h)_{e\mu}|$ which are by a factor 2×10^3 smaller and could set the limit:

$$|(h^\dagger h)_{e\mu}| < 3 \times 10^{-7} \left(\frac{m_{\Delta^+}}{100 \text{ GeV}} \right)^2. \quad (75)$$

4 TeV Scale Type III See-Saw Model

We turn in this section to the study of lepton flavour violating processes in type III see-saw [73] extensions of the SM. In the scenarios under discussion, the SM particle content is enlarged by adding $SU(2)_L$ -triplets of fermions, $\mathbf{F}_{jR} \equiv (F_{jR}^1, F_{jR}^2, F_{jR}^3)$, $j \geq 2$, possessing zero weak hypercharge and a mass M_k at the electroweak scale: $M_k \approx (100 - 1000)$ GeV. The corresponding interaction and mass terms in the see-saw Lagrangian read:

$$\mathcal{L}_{\text{seesaw}}^{\text{III}} = -\lambda_{\ell j} \bar{\psi}_{\ell L} \boldsymbol{\tau} \tilde{H} \cdot \mathbf{F}_{jR} - \frac{1}{2} (M_R)_{ij} \overline{\mathbf{F}}_{iL}^C \cdot \mathbf{F}_{jR} + \text{h.c.}, \quad (76)$$

where $\boldsymbol{\tau} \equiv (\tau^1, \tau^2, \tau^3)$, τ^a being the usual $SU(2)_L$ generators in the fundamental representation.

It is convenient in the following discussion to work with the charge eigenstates $F_{jR}^\pm \equiv (F_{jR}^1 \mp iF_{jR}^2)$ and $F_{jR}^0 \equiv F_{jR}^3$. Then, the physical states in the above Lagrangian correspond to electrically charged Dirac and neutral Majorana fermions, which are denoted as E_j and N_j , respectively: ¹⁰

$$E_j \equiv F_{jR}^- + F_{jL}^{+C} \quad N_j \equiv F_{jL}^{0C} + F_{jR}^0. \quad (77)$$

In the basis in which the charged lepton mass matrix is diagonal, the CC and NC weak interaction Lagrangian of the light Majorana neutrino mass eigenstates χ_j read:

$$\mathcal{L}_{CC}^\nu = -\frac{g}{\sqrt{2}} \bar{\ell} \gamma_\alpha ((1 - \eta)U)_{\ell i} \chi_{iL} W^\alpha + \text{h.c.}, \quad (78)$$

$$\mathcal{L}_{NC}^\nu = -\frac{g}{2c_w} \overline{\chi_{iL}} \gamma_\alpha (U^\dagger(1 + 2\eta)U)_{ij} \chi_{jL} Z^\alpha. \quad (79)$$

¹⁰In the following we will denote as E_j and N_j the mass eigenstates obtained from the diagonalization of the full charged and neutral lepton mass matrices.

Similarly to the type I see-saw scenario discussed earlier, the heavy Majorana mass eigenstates N_k might acquire a sizable coupling to the weak gauge bosons through the mixing with the light Majorana neutrinos:

$$\mathcal{L}_{CC}^N = \frac{g}{2\sqrt{2}} \bar{\ell} \gamma_\alpha (RV)_{\ell k} (1 - \gamma_5) N_k W^\alpha + \text{h.c.}, \quad (80)$$

$$\mathcal{L}_{NC}^N = -\frac{g}{4c_w} \bar{\nu}_\ell \gamma_\alpha (RV)_{\ell j} (1 - \gamma_5) N_j Z^\alpha + \text{h.c.} \quad (81)$$

In the expressions given above, the non-unitary part of the neutrino mixing matrix, *i.e.* the matrix η , and the matrix R are defined as in the type I see-saw scenario discussed in Section 2 (see eq. (13)), while V in this case diagonalizes the symmetric mass matrix M_R in eq. (76): $M_R \cong V^* \text{diag}(M_1, M_2, \dots) V^\dagger$.

The neutrino Yukawa couplings $\lambda_{\ell j}$ can be partially constrained by low-energy neutrino oscillation data and electroweak precision observable (see, *e.g.* [74, 75]). Notice that, unlike the type I see-saw extension of the Standard Model, now we have flavour changing neutral currents (FCNCs) in the charged lepton sector. The latter are described by the interaction Lagrangian:

$$\mathcal{L}_{NC}^\ell = \frac{g}{2c_w} (\bar{\ell}_L \gamma_\alpha (\mathbf{1} - 4\eta)_{\ell\ell'} \ell'_L - 2s_w^2 \bar{\ell} \gamma_\alpha \ell) Z^\alpha. \quad (82)$$

Finally,¹¹ the interactions of the new heavy charged leptons, E_j , with the weak gauge bosons at leading order in the mixing angle between the heavy and the light mass eigenstates read:

$$\mathcal{L}_{CC}^E = -g \bar{E}_j \gamma_\alpha N_j W^\alpha + g \bar{E}_j \gamma_\alpha (RV)_{\ell j} \nu_{\ell R}^C W^\alpha + \text{h.c.}, \quad (83)$$

$$\mathcal{L}_{NC}^E = g c_w \bar{E}_j \gamma_\alpha E_j Z^\alpha - \frac{g}{2\sqrt{2}c_w} (\bar{\ell} \gamma_\alpha (RV)_{\ell j} (1 - \gamma_5) E_j Z^\alpha + \text{h.c.}). \quad (84)$$

4.1 The $\mu \rightarrow e\gamma$ Decay

Charged lepton radiative decays receive additional contributions with respect to the scenario with singlet RH neutrinos, due to the presence of new lepton flavour violating interactions in the low energy effective Lagrangian (see eqs. (82) and (84)). Following the computation reported in [75], we have for the $\mu \rightarrow e\gamma$ decay branching ratio in the present scenario:

$$\text{BR}(\mu \rightarrow e\gamma) = \frac{3\alpha_{\text{em}}}{32\pi} |T|^2, \quad (85)$$

where the amplitude T is given by

$$T \cong -2 \left(\frac{13}{3} + \mathcal{C} \right) \eta_{\mu e} + \sum_k (RV)_{ek} (RV)_{\mu k}^* [A(x_k) + B(y_k) + C(z_k)], \quad (86)$$

¹¹Flavour changing couplings between the charged leptons and the SM Higgs boson H arise as well in the TeV-scale type III see-saw scenarios [75] which enter at one-loop in the lepton flavour violating processes (see next subsection).

with $x_k = (M_k/M_W)^2$, $y_k = (M_k/M_Z)^2$, $z_k = (M_k/M_H)^2$ and $\mathcal{C} \simeq -6.56$. The loop functions $A(x_k)$, $B(y_k)$ and $C(z_k)$ read [75]:

$$A(x) = \frac{-30 + 153x - 198x^2 + 75x^3 + 18(4-3x)x^2 \log x}{3(x-1)^4}, \quad (87)$$

$$B(y) = \frac{33 - 18y - 45y^2 + 30y^3 + 18(4-3y)y \log y}{3(y-1)^4}, \quad (88)$$

$$C(z) = \frac{-7 + 12z + 3z^2 - 8z^3 + 6(3z-2)z \log z}{3(z-1)^4}. \quad (89)$$

In the simple scenario of degenerate fermion triplets with an overall mass scale \overline{M} we obtain taking $M_H = 125$ GeV:

$$T/\eta_{\mu e} \cong 11.6 \text{ (5.2)}, \quad \text{for } \overline{M} = 100 \text{ (1000) GeV}. \quad (90)$$

For $\overline{M} = 100$ (1000) GeV, the current best upper limit on the $\mu \rightarrow e\gamma$ decay branching ratio obtained in the MEG experiment, eq. (3), implies the bound:

$$|\eta_{\mu e}| < 9 \text{ (20)} \times 10^{-6}, \quad \text{for } \overline{M} = 100 \text{ (1000) GeV}. \quad (91)$$

If no positive signal will be observed by the MEG experiment, that is if it results that $\text{BR}(\mu \rightarrow e\gamma) < 10^{-13}$, the following upper limit on the non-unitarity lepton flavour violating coupling $|\eta_{\mu e}|$ can be set:

$$|\eta_{\mu e}| < 2 \text{ (4)} \times 10^{-6}, \quad \text{for } \overline{M} = 100 \text{ (1000) GeV}. \quad (92)$$

4.2 The $\mu \rightarrow 3e$ and $\mu - e$ Conversion in Nuclei

The effective $\mu - e - Z$ effective coupling in the Lagrangian (82) provides the dominant contribution (at tree-level) to the $\mu \rightarrow 3e$ decay rate and the $\mu - e$ conversion rate in a nucleus. In the case of the first process we have (see, *e.g.*, [74]):

$$\text{BR}(\mu \rightarrow 3e) \simeq 16 |\eta_{\mu e}|^2 \left(3 \sin^4 \theta_W - 2 \sin^2 \theta_W + \frac{1}{2} \right). \quad (93)$$

Taking into account the experimental upper limit reported in (4), we get the following upper limit on the $\mu - e$ effective coupling:

$$|\eta_{\mu e}| < 5.6 \times 10^{-7}. \quad (94)$$

which is a stronger constraint with respect to the one derived from the non-observation of the $\mu \rightarrow e\gamma$ decay (see eqs. (92) and (91)), mediated (at one-loop) by an effective dipole operator.

More stringent constraints on the effective $\mu - e - Z$ coupling can be obtained using the data from the $\mu - e$ conversion experiments. Indeed, according to the general parametrisation given in [72] (see also [76, 75]), we have for the $\mu - e$ conversion ratio in a nucleus \mathcal{N} with N neutrons and Z protons:

$$\text{CR}(\mu \mathcal{N} \rightarrow e \mathcal{N}) \cong \frac{2 G_F^2}{\Gamma_{\text{capt}}} |\mathcal{C}_{\mu e}|^2 \left| (2 g_{LV(u)} + g_{LV(d)}) V^{(p)} + (g_{LV(u)} + 2 g_{LV(d)}) V^{(n)} \right|^2, \quad (95)$$

where in this case ¹²

$$\mathcal{C}_{\mu e} \equiv 4 \eta_{\mu e}, \quad (96)$$

$$V^{(n)} \simeq \frac{N}{Z} V^{(p)}, \quad g_{LV(u)} = 1 - \frac{8}{3} s_w^2 \quad \text{and} \quad g_{LV(d)} = -1 + \frac{4}{3} s_w^2. \quad (97)$$

An upper bound on $|\eta_{\mu e}|$ can be derived from the present experimental upper limit on the $\mu - e$ conversion rate in the nucleus of $^{48}_{22}\text{Ti}$, $\text{CR}(\mu \text{ Ti} \rightarrow e \text{ Ti}) \lesssim 4.3 \times 10^{-12}$. From eqs. (95)-(97) we get:

$$|\eta_{\mu e}| \lesssim 2.6 \times 10^{-7}. \quad (98)$$

If in the $\mu - e$ conversion experiments with $^{48}_{22}\text{Ti}$ the prospective sensitivity to $\text{CR}(\mu \text{ Ti} \rightarrow e \text{ Ti}) \sim 10^{-18}$ will be reached, these experiments will be able to probe values of $|\eta_{\mu e}|$ as small as $|\eta_{\mu e}| \sim 1.3 \times 10^{-10}$.

5 Discussion and Conclusions

We have performed a detailed analysis of charged lepton flavour violating (LFV) processes $-\mu \rightarrow e\gamma$, $\mu \rightarrow 3e$ and $\mu - e$ conversion in nuclei – in the context of see-saw type extensions of the Standard Model, in which the scale of new physics Λ is taken in the TeV range, $\Lambda \sim (100 - 1000) \text{ GeV}$. In this class of models, an effective Majorana mass term for the light left-handed active neutrinos is generated after electroweak symmetry breaking due to the decoupling of additional “heavy” scalar and/or fermion representations. We have analyzed in full generality the phenomenology of the three different and well-known (see-saw) mechanisms of neutrino mass generation, in their minimal formulation: *i*) type I see-saw models, in which the new particle content consist of at least 2 RH neutrinos, which are not charged under the SM gauge group; *ii*) type III see-saw models, where the RH neutrinos are taken in the adjoint representation of $SU(2)_L$ with zero hypercharge; *iii*) type II see-saw (or Higgs triplet) models, where the scalar sector of the theory is extended with the addition of at least one scalar triplet of $SU(2)_L$ coupled to charged leptons.

Under certain conditions the couplings of the SM charged leptons with the new fermions and/or scalars are, in principle, sizable enough to allow for their production and detection at present collider facilities, LHC included. On the other hand, remarkable indirect tests of such scenarios are also possible in ongoing and future experiments looking for charged lepton flavour violation. Indeed, the flavour structure of the interactions between the SM leptons and the new “heavy” particle states is mainly determined by the requirement of reproducing neutrino oscillation data, in such a way that the unknown parameter space can be expressed in terms of very few quantities. The latter can, therefore, be constrained by the measurement of different LFV observables. Further and complementary information is provided also by experiments which search for lepton number violating phenomena, such as neutrinoless double beta decays of even-even nuclei.

We summarize below the phenomenological implications of a possible observation of the LFV processes given above for each kind of (TeV scale) see-saw extensions of the SM.

¹²The expression for $V^{(n)}$ is valid under the assumption of equal proton and neutron number densities in the given nucleus [72]. The numerical value of the nuclear form factors for $^{48}_{22}\text{Ti}$, $^{27}_{13}\text{Al}$ and $^{197}_{79}\text{Au}$ is reported in Table 2.

Type I see-saw results. In this case the $\mu \rightarrow e\gamma$ and $\mu \rightarrow 3e$ decay branching ratios $\text{BR}(\mu \rightarrow e\gamma)$ and $\text{BR}(\mu \rightarrow 3e)$, and the $\mu-e$ conversion rate in a nucleus \mathcal{N} , $\text{CR}(\mu\mathcal{N} \rightarrow e\mathcal{N})$, $\mathcal{N} = \text{Al, Ti, Au}$, can have values close to the existing upper limits and within the sensitivity of the ongoing MEG experiment searching for the $\mu \rightarrow e\gamma$ decay and the future planned $\mu-e$ conversion and $\mu \rightarrow 3e$ decay experiments [29, 30, 31, 32, 33]. The relevant LFV observable in the minimal scenario, with the addition of only two RH neutrinos to the SM particle content, is provided by the quantity $|(RV)_{\mu 1}^*(RV)_{e 1}|$, where $(RV)_{\ell j}$ ($j = 1, 2$) denote the couplings of the fermion singlets to the SM charged leptons (see eqs. (15) and (16)). If the MEG experiment reaches the projected sensitivity and no positive signal will be observed implying that $\text{BR}(\mu \rightarrow e\gamma) < 10^{-13}$, there still will be a relatively large interval of values of $|(RV)_{\mu 1}^*(RV)_{e 1}|$, as Fig. 2 shows, for which the $\mu-e$ conversion and $\mu \rightarrow 3e$ decay are predicted to have observable rates in the planned next generation of experiments.

It follows from the analysis performed by us that as a consequence of an accidental cancellation between the contributions due to the different one loop diagrams in the $\mu-e$ conversion amplitude, the rate of $\mu-e$ conversion in Al and Ti or in Au can be strongly suppressed for certain values of the see-saw scale M_1 . As we have seen, this suppression can be efficient either for the conversion in Al and Ti or for the conversion in Au, but not for all the three nuclei, the reason being that the values of M_1 for which it happens in Al and Ti differ significantly from those for which it occurs in Au. In both the cases of Al or Ti and Au, the suppression can be effective only for values of M_1 lying in very narrow intervals (see Figs. 3 and 4).

In the case of IH light neutrino mass spectrum, all the three LFV observables, $\text{BR}(\mu \rightarrow e\gamma)$, $\text{BR}(\mu \rightarrow 3e)$ and $\text{CR}(\mu\mathcal{N} \rightarrow e\mathcal{N})$, can be strongly suppressed due to the fact that the LFV factor $|(RV)_{\mu 1}|^2 \propto |U_{\mu 2} + i\sqrt{m_1/m_2}U_{\mu 1}|^2 \cong |U_{\mu 2} + iU_{\mu 1}|^2$, in the expressions of the three rates can be exceedingly small. This requires a special relation between the Dirac and the Majorana CPV phases δ and α_{21} , as well as between the neutrino mixing angle θ_{13} and the phase δ (see eq. (34)). For the values of $\sin\theta_{13}$ from the current 3σ allowed interval, eq. (1), one can have $|U_{\mu 2} + iU_{\mu 1}|^2 \cong 0$ provided $0 \leq \delta \lesssim 0.7$. *A priori* it is not clear why the relations between δ and α_{21} , and between δ and θ_{13} , leading to $|U_{\mu 2} + iU_{\mu 1}|^2 = 0$, should take place (although, in general, it might be a consequence of the existence of an approximate symmetry). The suppression under discussion cannot hold if, for instance, it is experimentally established that δ is definitely bigger than 1.0. That would be the case if the existing indications [9] that $\cos\delta < 0$ receive unambiguous confirmation.

We note finally that for $M_1 \gtrsim 100$ GeV we have: $\text{BR}(\mu \rightarrow 3e)/\text{BR}(\mu \rightarrow e\gamma) \gtrsim 0.067$. Thus, if it is experimentally established that $\text{BR}(\mu \rightarrow 3e)/\text{BR}(\mu \rightarrow e\gamma)$ is much smaller than the quoted lower bound, the model considered with $M_1 \gtrsim 100$ GeV will be ruled out. Such a result would be consistent also just with a see-saw scale $M_1 < 100$ GeV.

Type II see-saw results. It follows from the results obtained in Section 3 that the predictions for the $\mu \rightarrow e\gamma$ and $\mu \rightarrow 3e$ decay branching ratios, as well as the $\mu-e$ conversion rate in a nucleus \mathcal{N} , in the TeV scale type II see-saw scenario considered exhibit, in general, different dependence on the masses of the singly- and doubly-charged Higgs particles Δ^+ and Δ^{++} , which mediate (to leading order) the three processes. For $m_{\Delta^+} \cong m_{\Delta^{++}} \cong M_\Delta$, all the three rates are proportional to M_Δ^{-4} , i.e., they diminish as the 4th power of the see-saw scale when the latter increases.

The matrix of Yukawa couplings $h_{\ell\ell'}$ which are responsible for the LFV processes of

interest, is directly related to the neutrino Majorana mass matrix and thus to the PMNS neutrino mixing matrix U . As a consequence, $\text{BR}(\mu \rightarrow e\gamma)$, $\text{BR}(\mu \rightarrow 3e)$ and $\text{CR}(\mu\mathcal{N} \rightarrow e\mathcal{N})$ depend, in general, on the neutrino mass and mixing parameters, including the CPV phases in U .

To be more specific, $\text{BR}(\mu \rightarrow e\gamma)$ does not depend on the Majorana CPV phases and on $\min(m_j)$, and its dependence on the Dirac CPV phase and on the type of neutrino mass spectrum is insignificant. In contrast, both $\text{BR}(\mu \rightarrow 3e)$ and $\text{CR}(\mu\mathcal{N} \rightarrow e\mathcal{N})$ exhibit very strong dependence on the type of neutrino mass spectrum and on the values of the Majorana and Dirac CPV phases. As a consequence, the predictions for $\text{BR}(\mu \rightarrow 3e)$ and $\text{CR}(\mu\mathcal{N} \rightarrow e\mathcal{N})$ for given M_Δ can vary by several orders of magnitude not only when the spectrum changes from NH (IH) to QD as a function of the lightest neutrino mass, but also when one varies only the values of the CPV phases keeping the type of the neutrino mass spectrum fixed. All the three observables under discussion can have values within the sensitivity of the currently running MEG experiment on the $\mu \rightarrow e\gamma$ decay and the planned future experiments on the $\mu \rightarrow 3e$ decay and $\mu - e$ conversion. However, for a given see-saw scale in the range of $\sim (100 - 1000)$ GeV, the planned experiments on $\mu - e$ conversion in Al or Ti will provide the most sensitive probe of the LFV Yukawa couplings of the TeV scale type II see-saw model.

Type III see-saw results. Unlike the type I see-saw extension of the SM discussed in Section 2, in this scenario we have several – possibly sizable – lepton flavour violating interactions in the low energy effective Lagrangian, due to the higher $SU(2)_L$ representation of the new fermion fields. In particular, FCNCs arise at tree-level from the non-unitarity of the PMNS matrix (see eq. (82)). Thus, the effective $\mu - e - Z$ coupling in (82) makes it possible an enhancement of at least two orders of magnitude of the rates of $\mu \rightarrow e\gamma$, $\mu \rightarrow 3e$ and $\mu - e$ conversion with respect to the ones predicted in the type I see-saw scenario, with RH neutrinos taken in the TeV range. Consequently, all the predicted LFV observables may be probed in the related present and future experiments. As in the previous scenarios, the strongest constraint on the flavour structure of this class of models is by far provided by the expected very high sensitivity reach of $\mu - e$ conversion experiments.

In conclusion, the oncoming combination of data on neutrino oscillations, collider searches and lepton number/flavour violating processes represent an important opportunity to reveal in the next future the fundamental mechanism at the basis of the generation of neutrino masses as well as the underlying physics beyond the standard theory.

Acknowledgments

This work was supported in part by the INFN program on “Astroparticle Physics”, by the Italian MIUR program on “Neutrinos, Dark Matter and Dark Energy in the Era of LHC” (D.N.D. and S.T.P.) and by the World Premier International Research Center Initiative (WPI Initiative), MEXT, Japan (S.T.P.), by the DFG cluster of excellence “Origin and Structure of the Universe” and the ERC Advanced Grant project “FLAVOUR” (267104) (A.I.), and by the Fundação para a Ciência e a Tecnologia (FCT, Portugal) through the projects PTDC/FIS/098188/2008, CERN/FP/116328/2010 and CFTP-FCT Unit 777, which are

partially funded through POCTI (FEDER) (E.M.).

References

- [1] K. Nakamura and S.T. Petcov, “Neutrino Mass, Mixing, and Oscillations”, in K. Nakamura et al. (Particle Data Group), J. Phys. G **37** (2010) 075021.
- [2] Y. Fukuda *et al.* [Super-Kamiokande Collaboration], Phys. Rev. Lett. **81** (1998) 1562 [hep-ex/9807003].
- [3] Q.R. Ahmad *et al.* [SNO Collaboration], Phys. Rev. Lett. **87** (2001) 071301.
- [4] Y. Fukuda *et al.* [Super-Kamiokande Collaboration], Phys. Rev. Lett. **86** (2001) 5651.
- [5] K. Eguchi *et al.* [KamLAND Collaboration], Phys. Rev. Lett. **90** (2003) 021802 [arXiv:hep-ex/0212021].
- [6] K. Abe *et al.* [T2K Collaboration], Phys. Rev. Lett. **107** (2011) 041801 [arXiv:1106.2822].
- [7] P. Adamson *et al.* [MINOS Collaboration], Phys. Rev. Lett. **107** (2011) 181802.
- [8] Y. Abe *et al.* [Double Chooz Collaboration], arXiv:1112.6353.
- [9] G. L. Fogli *et al.*, Phys. Rev. D **84** 053007 (2011).
- [10] T. Schwetz, M Tórtola, and J.W.F. Valle, New J. Phys. **13** (2011) 109401.
- [11] F.P. An *et al.* [Daya Bay Collaboration], arXiv:1203.1669.
- [12] J.K. Ahn *et al.* [RENO Collaboration], arXiv:1204.0626.
- [13] K. Schreckenbach *et al.*, Phys. Lett. B **160** (1985) 325.
- [14] G. Mention *et al.*, Phys. Rev. D **83** (2011) 073008.
- [15] J. Bernabéu, S. Palomares-Ruiz and S.T. Petcov, Nucl. Phys. B **669** (2003) 255; S. Palomares-Ruiz and S.T. Petcov, Nucl. Phys. **B712** (2005) 392; S.T. Petcov and T. Schwetz, *ibid.* B **740** (2006) 1; R. Gandhi *et al.*, Phys. Rev. D **76** (2007) 073012 [arXiv:0707.1723 [hep-ph]].
- [16] S.T. Petcov and M. Piai, Phys. Lett. B **533** (2002) 94; S. Choubey, S.T. Petcov and M. Piai, Phys. Rev. D **68** (2003) 113006; P. Ghoshal and S.T. Petcov, JHEP **1103** (2011) 058, and references quoted therein.
- [17] S. Pascoli and S. T. Petcov, Phys. Rev. D **77** (2008) 113003.
- [18] S. Pascoli, S.T. Petcov and A. Riotto, Phys. Rev. D **75** (2007) 083511, and Nucl. Phys. B **774** (2007) 1.
- [19] E. Molinaro and S.T. Petcov, Phys. Lett. B **671** (2009) 60.

- [20] J. Adam *et al.* [MEG Collaboration], Phys. Rev. Lett. **107** (2011) 171801 [arXiv:1107.5547 [hep-ex]].
- [21] U. Bellgardt *et al.* [SINDRUM Collaboration], Nucl. Phys. B **299** (1988) 1.
- [22] C. Dohmen *et al.* [SINDRUM II Collaboration.], Phys. Lett. B **317** (1993) 631.
- [23] B. Aubert *et al.* [BABAR Collaboration], Phys. Rev. Lett. **104** (2010) 021802 [arXiv:0908.2381 [hep-ex]].
- [24] M. Raidal, A. Strumia and K. Turzyski, Phys. Lett. B **609** (2005) 351 [Erratum-ibid. B **632** (2006) 752] [hep-ph/0408015].
- [25] M. Shaposhnikov, Nucl. Phys. B **763** (2007) 49 [hep-ph/0605047].
- [26] J. Kersten and A. Y. Smirnov, Phys. Rev. D **76** (2007) 073005 [arXiv:0705.3221 [hep-ph]].
- [27] M. B. Gavela, T. Hambye, D. Hernandez and P. Hernandez, JHEP **0909** (2009) 038 [arXiv:0906.1461 [hep-ph]].
- [28] A. Ibarra, E. Molinaro and S. T. Petcov, Phys. Rev. D **84** (2011) 013005 [arXiv:1103.6217 [hep-ph]].
- [29] See, e.g., <http://comet.phys.sci.osaka-u.ac.jp/>.
- [30] See, e.g., <http://mu2e.fnal.gov/>.
- [31] Y. Mori *et al.* [The PRIME Working Group], “An Experimental Search for $\mu^- \rightarrow e^-$ Conversion Process at an Ultimate Sensitivity of the Order of 10^{-18} with PRISM”, LOI-25.
- [32] See, e.g., <http://projectx.fnal.gov/>.
- [33] This is part of the program of research planned to be realised with the MuSIC facility at Osaka University, Japan (private communication by Y. Kuno).
- [34] A. G. Akeroyd *et al.* [SuperKEKB Physics Working Group Collaboration], hep-ex/0406071.
- [35] M. Bona *et al.* [SuperB Collaboration], Pisa, Italy: INFN (2007) 453 p. www.pi.infn.it/SuperB/?q=CDR [arXiv:0709.0451 [hep-ex]].
- [36] P. Minkowski, Phys. Lett. B **67** (1977) 421; M. Gell-Mann, P. Ramond and R. Slansky, *Proceedings of the Supergravity Stony Brook Workshop*, New York 1979, eds. P. Van Nieuwenhuizen and D. Freedman; T. Yanagida, *Proceedings of the Workshop on Unified Theories and Baryon Number in the Universe*, Tsukuba, Japan 1979, eds. A. Sawada and A. Sugamoto; R. N. Mohapatra and G. Senjanovic, Phys. Rev. Lett. **44** (1980) 912.
- [37] A. Ibarra, E. Molinaro and S. T. Petcov, JHEP **1009** (2010) 108 [arXiv:1007.2378 [hep-ph]].

- [38] B. Pontecorvo, Zh. Eksp. Teor. Fiz. (JETP) **33** (1957) 549, **34** (1958) 247 and **53** (1967) 1717.
- [39] Z. Maki, M. Nakagawa and S. Sakata, Prog. Theor. Phys. **28** (1962) 870.
- [40] S. Antusch, J. P. Baumann and E. Fernandez-Martinez, Nucl. Phys. B **810** (2009) 369 [arXiv:0807.1003 [hep-ph]].
- [41] S. Antusch *et al.*, JHEP **0610** (2006) 084 [arXiv:hep-ph/0607020].
- [42] A. Merle and W. Rodejohann, Phys. Rev. D **73** (2006) 073012.
- [43] A. Kleppe, “*Extending The Standard Model With Two Right-Handed Neutrinos*”, in **Lohusaku 1995, Neutrino physics**, 118-125; E. Ma, D. P. Roy and U. Sarkar, Phys. Lett. B **444** (1998) 391; P. H. Frampton, S. L. Glashow and T. Yanagida, Phys. Lett. B **548** (2002) 119 [arXiv:hep-ph/0208157]; M. Raidal and A. Strumia, Phys. Lett. B **553**, 72 (2003) [arXiv:hep-ph/0210021]; V. Barger, D. A. Dicus, H. J. He and T. j. Li, Phys. Lett. B **583** (2004) 173 [arXiv:hep-ph/0310278]. T. Endoh, S. Kaneko, S. K. Kang, T. Morozumi and M. Tanimoto, Phys. Rev. Lett. **89** (2002) 231601 [arXiv:hep-ph/0209020].
- [44] A. Ibarra and G. G. Ross, Phys. Lett. B **591** (2004) 285 [arXiv:hep-ph/0312138]; Phys. Lett. B **575** (2003) 279 [arXiv:hep-ph/0307051].
- [45] S. T. Petcov, W. Rodejohann, T. Shindou and Y. Takanishi, Nucl. Phys. B **739** (2006) 208 [arXiv:hep-ph/0510404].
- [46] L. Wolfenstein, Nucl. Phys. B **186** (1981) 147.
- [47] S.T. Petcov, Phys. Lett. B **110** (1982) 245.
- [48] S.M. Bilenky, J. Hosek and S.T. Petcov, Phys. Lett. B **94** (1980) 495.
- [49] M. L. Brooks *et al.* [MEGA Collaboration], Phys. Rev. Lett. **83** (1999) 1521 [arXiv:hep-ex/9905013].
- [50] S. T. Petcov, Sov. J. Nucl. Phys. **25** (1977) 340 [Yad. Fiz. **25** (1977) 641]; S.M. Bilenky, S.T. Petcov and B. Pontecorvo, Phys. Lett. B **67** (1977) 309.
- [51] T. P. Cheng and L. F. Li, Phys. Rev. Lett. **45** (1980) 1908.
- [52] J. Hisano *et al.*, Phys. Rev. D **53** (1996) 2442.
- [53] A. J. Buras, B. Duling, T. Feldmann, T. Heidsieck and C. Promberger, JHEP **1009** (2010) 104 [arXiv:1006.5356 [hep-ph]].
- [54] J. Hisano and K. Tobe, Phys. Lett. B **510** (2001) 197.
- [55] M. Magg and C. Wetterich, Phys. Lett. B **94** (1980) 61; J. Schechter and J. W. F. Valle, Phys. Rev. D **22** (1980) 2227; R. N. Mohapatra and G. Senjanovic, Phys. Rev. D **23** (1981) 165.

- [56] M. Kakizaki, Y. Ogura and F. Shima, Phys. Lett. B **566** (2003) 210 [arXiv:hep-ph/0304254]; A. G. Akeroyd, M. Aoki and H. Sugiyama, Phys. Rev. D **79** (2009) 113010 [arXiv:0904.3640 [hep-ph]].
- [57] T. Han, B. Zhang, Phys. Rev. Lett. **97** (2006) 171804 [hep-ph/0604064]. F. del Aguila, J. A. Aguilar-Saavedra, R. Pittau, JHEP **0710** (2007) 047 [hep-ph/0703261]. A. Atre *et al.*, JHEP **0905** (2009) 030; F. del Aguila, J. A. Aguilar-Saavedra, Nucl. Phys. **B813** (2009) 22-90. [arXiv:0808.2468 [hep-ph]].
- [58] A. G. Akeroyd, S. Moretti and H. Sugiyama, Phys. Rev. D **85**, 055026 (2012) [arXiv:1201.5047 [hep-ph]].
- [59] E. J. Chun, K. Y. Lee and S. C. Park, Phys. Lett. B **566**, 142 (2003) [arXiv:hep-ph/0304069].
- [60] M. C. Chen, Phys. Rev. D **71**, 113010 (2005) [arXiv:hep-ph/0504158].
- [61] E. Ma, M. Raidal and U. Sarkar, Phys. Rev. Lett. **85** (2000) 3769, and Nucl. Phys. B **615** (2001) 313; A. G. Akeroyd and C. W. Chiang, Phys. Rev. D **81** (2010) 115007.
- [62] J. Bernabeu, A. Pich and A. Santamaria, Z. Phys. C **30** (1986) 213; G.K. Leontaris, K. Tamvakis and J.D. Vergados, Phys. Lett. B **162** (1985) 153.
- [63] M. Raidal and A. Santamaria, Phys. Lett. B **421** (1998) 250 [arXiv:hep-ph/9710389]; E. Ma, M. Raidal and U. Sarkar, Nucl. Phys. B **615** (2001) 313 [arXiv:hep-ph/0012101].
- [64] S.T. Petcov, Phys. Lett. B **115** (1982) 401.
- [65] S. M. Bilenky and S. T. Petcov, Rev. Mod. Phys. **59** (1987) 671.
- [66] S.M. Bilenky, S. Pascoli and S.T. Petcov, Phys. Rev. D **64** (2001) 053010; S.T. Petcov, Physica Scripta T **121** (2005) 94 and Int. J. Mod. Phys A **25** (2010) 4325.
- [67] S.T. Petcov, H. Sugiyama and Y. Takanishi, Phys. Rev. D **80** (2009) 015005.
- [68] H.V. Klapdor-Kleingrothaus *et al.*, Phys. Lett. B **586** (2004) 198.
- [69] H.V. Klapdor-Kleingrothaus *et al.*, Mod. Phys. Lett. A **16** (2001) 2409.
- [70] W. Rodejohann, Int. J. Mod. Phys. E **20** (2011) 1833.
- [71] S. Pascoli and S.T. Petcov, Phys. Lett. B **544** (2002) 239; *ibid.* **580** (2004) 280.
- [72] R. Kitano, M. Koike and Y. Okada, Phys. Rev. D **66** (2002) 096002 [Erratum-*ibid.* D **76** (2007) 059902] [arXiv:hep-ph/0203110].
- [73] R. Foot, H. Lew, X. G. He and G. C. Joshi, Z. Phys. C **44** (1989) 441. E. Ma, Phys. Rev. Lett. **81** (1998) 1171 [arXiv:hep-ph/9805219].
- [74] A. Abada, C. Biggio, F. Bonnet, M. B. Gavela and T. Hambye, JHEP **0712** (2007) 061 [arXiv:0707.4058 [hep-ph]].

- [75] A. Abada, C. Biggio, F. Bonnet, M. B. Gavela, T. Hambye, Phys. Rev. **D78** (2008) 033007. [arXiv:0803.0481 [hep-ph]].
- [76] J. Bernabeu, E. Nardi, D. Tommasini, Nucl. Phys. **B409** (1993) 69-86. [hep-ph/9306251].